Mineralia Slovaca, Web ISSN 1338-3523, ISSN 0369-2086, https://doi.org/10.56623/ms.2022.54.2.1
54, 2 (2022), 95 – 118, © Authors 2022. CC BY 4.0

Results of the second phase of deep-sea polymetallic nodules geological survey in Interoceanmetal Joint Organization licence area (2016–2021)

PETER BALÁŽ

Interoceanmetal Joint Organization, Szczecin, Poland

Abstract: The exploration rights of the Interoceanmetal Joint Organization for exploration of polymetallic nodules (PMN) are granted from 29 March 2001 to an area located within the Clarion-Clipperton Zone (CCZ) in the eastern central Pacific Ocean. Exploration area covers 75,000 km^2 and consists of two sectors (B1 and B2). The B2 sector comprises four exploration blocks (H11, H22, H33 and H44). The most prospective area, selected for detailed research, is marked as H22_NE exploitable block and delineated within the H22 exploration block. The article presents results of geological survey, based mostly on the data collected during the second phase of exploration in the licence area (2016–2021, extension of the contract). Results are based on IOM's expeditions and relevant analytical work. During the IOM-2018 expedition high resolution bathymetric survey of H11, H22, H33 and H44 exploration blocks was carried out. The IOM-2019 expedition provided a new set of the data obtained using the distance methods (side-scan sonar, profiler) and contact methods (box-corer and gravity corer) in H22_NE exploitable block, H33 exploration block and preliminary delineated Preservation Reference Zone. The study was focused on analytical work based on sediment and nodule analyses of samples in H22 exploration block and H22_NE exploitation block. New estimation of mineral resources in B2 sector was caried out using the geostatistical method of ordinary block kriging with Yamamoto correction. The polymetallic nodule resources have been classified within the Inferred, Indicated and Measured Resources categories of the CRIRSCO classification system.

Key words: deep sea exploration, seabed minerals, polymetallic nodules, Clarion-Clipperton Zone

Graphical abstract

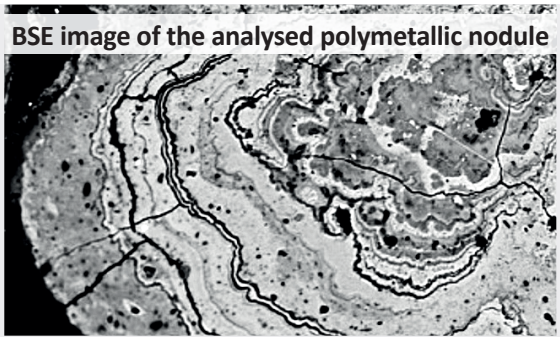

Highlights

- Detailed multibeam bathymetry mapping of 4 exploration blocks (H11, H22, H33, H44).
- Chemical, geochemical and mineralogical analysis of sediments and nodules in H22_NE block.
- Assessment of the ability to determine polymetallic nodule abundance based on seabed photography.
- New resource estimate, including identification of Measured Resources (CRIRSCO classification system).

Introduction

The exploration rights of the Interoceanmetal Joint Organization are granted from 29 March 2001 to an area located within the Clarion-Clipperton Zone (CCZ) in the eastern central Pacific Ocean. All activities related to exploration of minerals in the CCZ (the Area – the seabed and ocean floor beyond the limits of national jurisdiction) come under the United Nations Convention on the Law of the Sea (1982), the Agreement relating to the implementation of Part XI of the Convention (1994) as well as Regulations on Prospecting and Exploration for Polymetallic Nodules in the Area – regulations established by the International Seabed Authority (ISA). The ISA issues legal documents regulating the conduct of research and the future use of the seabed.

As of 2021, ISA has entered into 19 contracts for exploration for polymetallic nodules (PMN) in the Clarion-Clipperton Fracture Zone, Central Indian Ocean Basin and Western Pacific Ocean. Besides that, there were 7 contracts for exploration for polymetallic sulphides in the South West Indian Ridge, Central Indian Ridge and the Mid-Atlantic Ridge and 5 contracts for exploration for cobalt-rich crusts in the Western Pacific Ocean (ISA, 09/2021).

Adjacent properties (common borders) to the IOM exploration area belong to 4 organizations – NORI (Nauru), OMS (Singapore), BGR (Germany) and BMJ (Jamaica) (Fig. 1). The BMJ exploration area was delineated in April 2021 and reflects generally increased interest in deep sea mineral exploration in the area that has emerged during the past decade. 11 out of a total 19 exploration contracts has been signed in the 2011–2021 period.

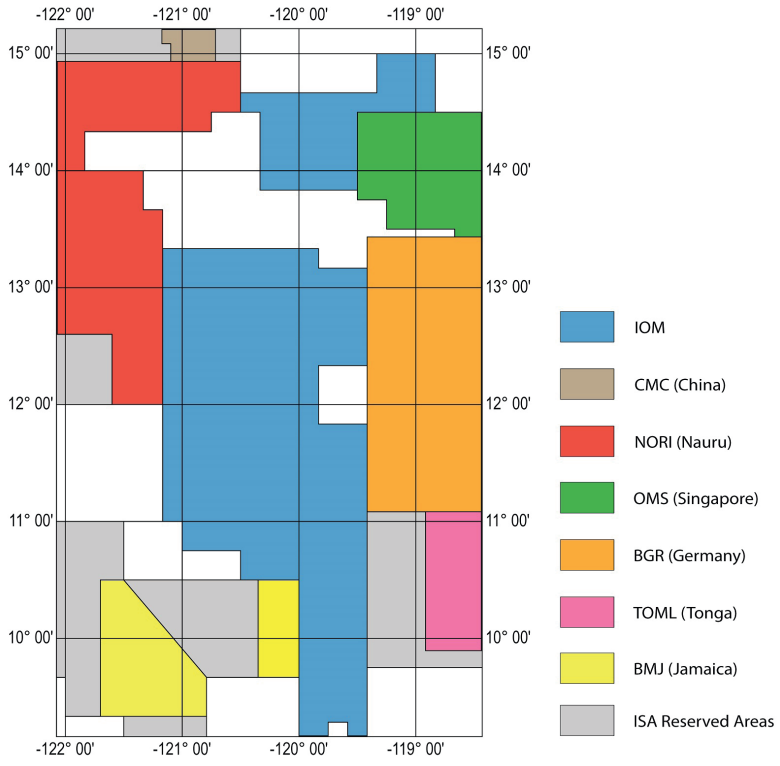

Fig. 1. Outlines of the IOM exploration area and adjacent properties in the Clarion-Clipperton Zone (ISA, 2021).

The IOM's contract for exploration of polymetallic nodules was granted for 15 years and provides the contractor security of tenure and exclusive right to explore for polymetallic nodules in the exploration area, as well as to move to a contract for exploitation. Regulations for exploitation of mineral resources in the Area are under the development process by the ISA. In 2016, the contract was extended for the following 5 years. A summary of the results of the geological survey of the first phase (2001–2016) was published recently (Baláž, 2021).

In addition to geological survey, IOM is engaged in research into the technology of mining and processing of deep-sea polymetallic nodules, as well as environmental research.

Location

The IOM exploration area covers app. 75,000 km^2 of the eastern part of the CCZ and consists of two sectors, B1 and B2. In B2 sector there are four exploration blocks (H11, H22, H33, H44) and preliminary delineated Preservation Reference Zone (Tab. 1, Fig. 2). Within the H22 exploration block the H22_NE exploitable block was delineated. Preservation Reference Zone (PRZ) is an area in which no mining shall occur to ensure representative and stable biota of the seabed in order to assess any changes of the marine environment. The obligation of establishing the PRZ in its license area is imposed on the contractor by the ISA. Delineation of the PRZ in the IOM exploration area is preliminary and the final location is being considered.

Tab. 1

IOM's Exploration area (sectors and blocks). Areas are calculated in UTM map projection coordinate system.

Exploration area	Area [km^2]
B1 sector	11 952
B2 sector	63 234
H11 exploration block	5 390
H22 exploration block	4 151
H22_NE exploitable block	957
H33 exploration block	4 008
H44 exploration block	1 919
PRZ (preliminary)	2 626
Total	**75 186**

Survey methodology

Before the signing of the exploration contract between the ISA and IOM in 2001, 21 research expeditions were carried out to the CCZ area, mainly focused on regional research. In the first phase of the contract (2001–2016), 4 expeditions were organized. In the second phase (2016–2021, the extension of the contract) there were 2 expeditions. The work was carried out in accordance with the program approved by the ISA. The study included a geological survey focused on determination of PMN abundance, nodule coverage, determination of metal content and chemical composition of PMNs, as well as study of seabed sediments, their geotechnical properties. During the expeditions basic oceanographic, meteorological and environmental data were collected. During the extension period 2 expeditions were carried out (2018 and 2019):

IOM-2018

- high resolution bathymetric mapping of selected parts of the IOM exploration area – H11, H22, H33 and H44 exploration blocks (15 609 km^2 in total),
- H11 5,400 km^2 (1 : 100 000 scale),
- H22 3,201 km^2 (1 : 100 000),
- H33 3,970 km^2 (1 : 100 000),
- H44 1,920 km^2 (1 : 100 000),
- H22_NE 1,118 km^2 (1 : 50 000).

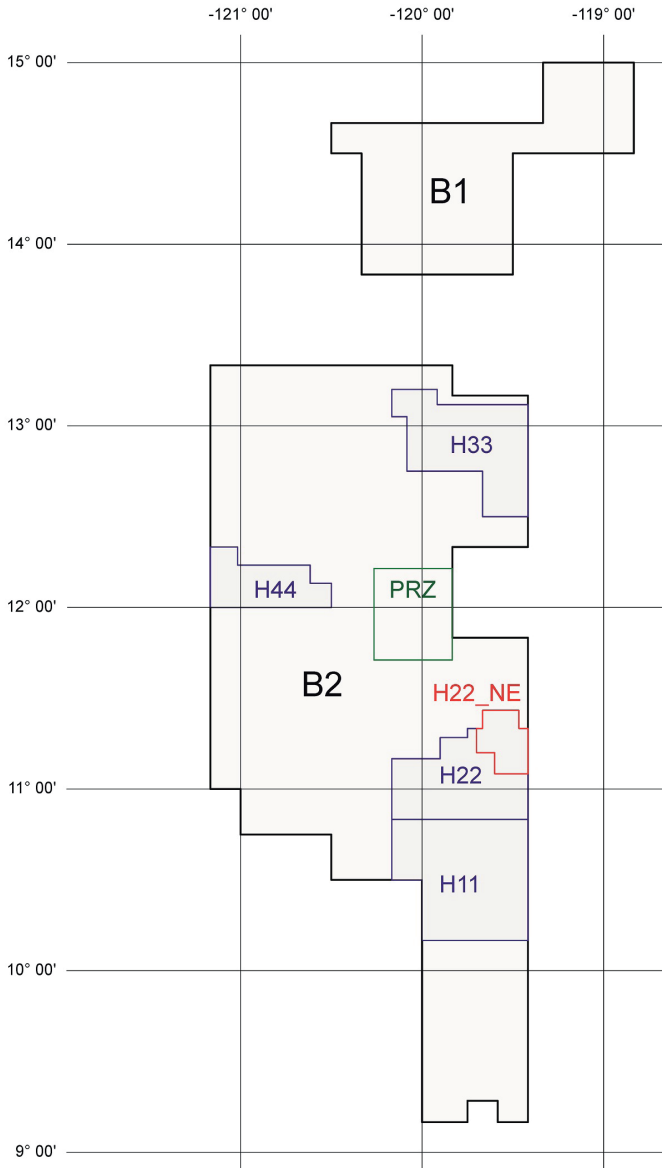

Fig. 2. IOM exploration area (B1 and B2 – sectors, H11, H22, H33, H44 – exploration blocks, H22_NE – exploitable block, PRZ – Preservation Reference Zone).

Multibeam bathymetry was used to measure depth and map the bottom morphology using multibeam echo sounder, providing information on the character of the seabed based on the intensity of the reflected signal (backscatter). Work was carried out in exploration blocks H11, H22, H33 and H44. A detailed survey was carried out in the H22_NE exploitable block.

IOM-2019

IOM conducted an at-sea exploration in selected parts of the exploration area (H22_NE exploitable block, H33 exploration block and Preservation Reference Zone).

- Geoacoustic profiling 313.54 km
- Photo-video profiling 418.14 km
- Sample retrieval with a box corer 32 launch-raising operations
- Sample retrieval with a gravity corer 4 launch-raising operations

As a part of the IOM-2019 expedition, geoacoustic survey (geoacoustic profiling with side-scan sonar) was used for detailed mapping of the seabed, obtaining the acoustic bottom profile to a depth of about 100 m. Photo and video profiling provided information for the analysis of bottom nodule coverage (individual images of the bottom) and the identification of zones with the occurrence of PMN, as well as the identification of obstacles to potential mining. Two types of seabed sampling systems were applied during the expeditions: sampling of PMN and sediments using a box-corer device; and sediment sampling using a gravity-corer device. Basic work and measurements requiring immediate sample processing were performed on board of the research vessel during the shipment.

Results

After individual expeditions, the results of the survey were summarized in reports on geological and environmental research, in semi-annual reports for the meetings of the IOM Council, as well as in annual reports for the ISA. The overview and results of the survey work are summarized in technical reports (Baláž et al., 2019; Zarzecki et al., 2021).

The presented results provide additional information to the data presented earlier (Baláž, 2021), relevant for updating the resources estimate in the B2 sector. The collected data are used for planning of the IOM polymetallic nodules project – potential exploitation and processing of raw materials, environmental impact assessment, economic assumptions and feasibility of the project.

Seabed topography

The bathymetric survey was carried out according to the design profile scheme. Exploration blocks H11, H22, H33 and H44 were mapped at scale 1 : 100 000. A system of parallel profiles has been used, to ensure 80 % overlap of adjacent profiles. The distance between profiles was 9 km. Exploitable block N22_NE was mapped at scale 1 : 50 000. A system of parallel profiles has been used, to ensure 100 % overlap of adjacent profiles. The distance between the profiles was 4.3 km. This provides detailed information for the area selected for initial mining phases.

A set of charts were prepared for each block, including the colour-shade chart (Fig. 3), the bathymetric chart with

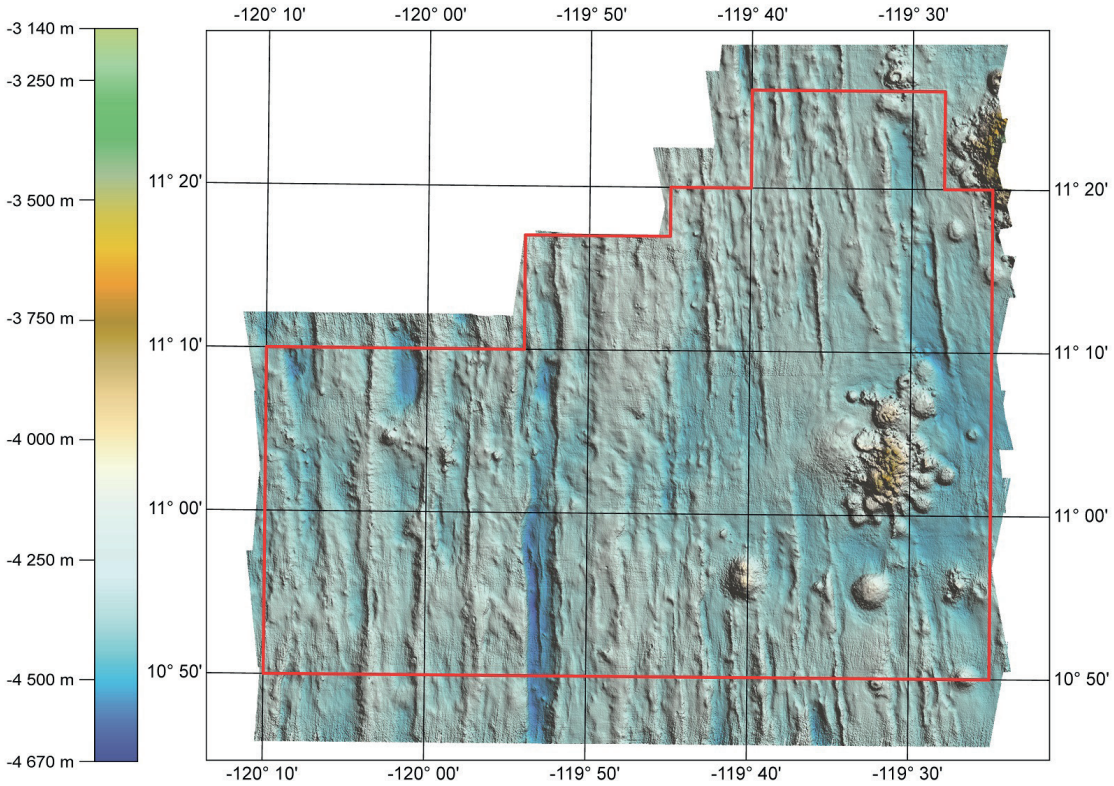

Fig. 3. Colour-shade chart of the H22 exploration block.

contours, the contours chart, the gradient chart, the chart of slopes of the sea-bottom exceeding 7° as well as the chart of amplitudes of the backscattered signal.

Lithology and stratigraphy

The structure of the sedimentary cover of the H22 exploration block

The study of the structure of the sedimentary cover of exploration block H22 is based on the interpretation of hydroacoustic profile 707_2. The total length of the profile is 57,159 m. It is a continuation of the hydroacoustic profile No. 707, passing from the south from the H11 exploration block. The profile is oriented from SW to NE, azimuth 65° (Fig. 4).

Hydroacoustic complex A is subdivided into subcomplexes A1 and A2, where A1 includes cover clay and siliceous-clayey sediments and A2 clay sediments – red deep-sea clays, radiolarian clays, possibly with zeolites. The acoustic boundaries between A1 and A2 are discontinuous and are clearly manifested only in those sections where clay-ore crusts with increased strength characteristics are found in the upper part of red deep-sea clays, which are a good acoustic marker. Complex B represents calcareous clays, an interbedding of nanofossil limestones and radiolarian clays, complex C represents layer of nanofossil limestones and complex F represents basement, composed of tholeiitic basalt (Fig. 5). A study shows that the maximum thickness of the sedimentary cover in the full section is 92 m at the 17.2 km picket. Thickness of particular hydroacoustic complexes: A1 – 6.5 m, A2 – 11 m, B – 39.3 m, C – 35.2 m (Dreiseitl, 2018).

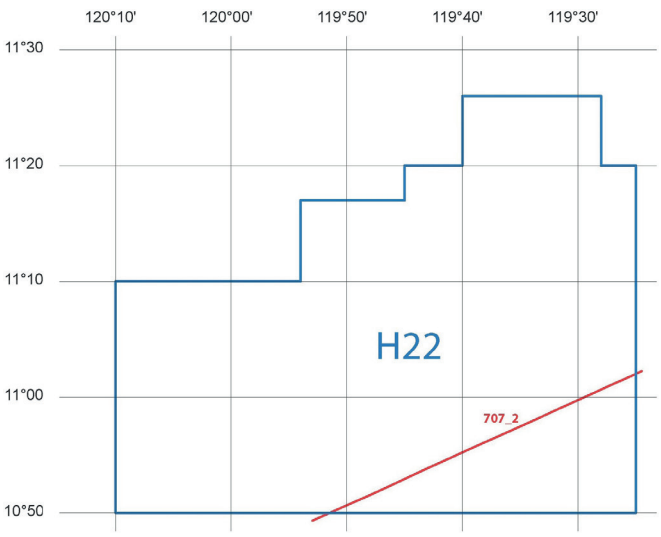

Fig. 4. Position of the 707_2 profile in the H22 exploration block (red line).

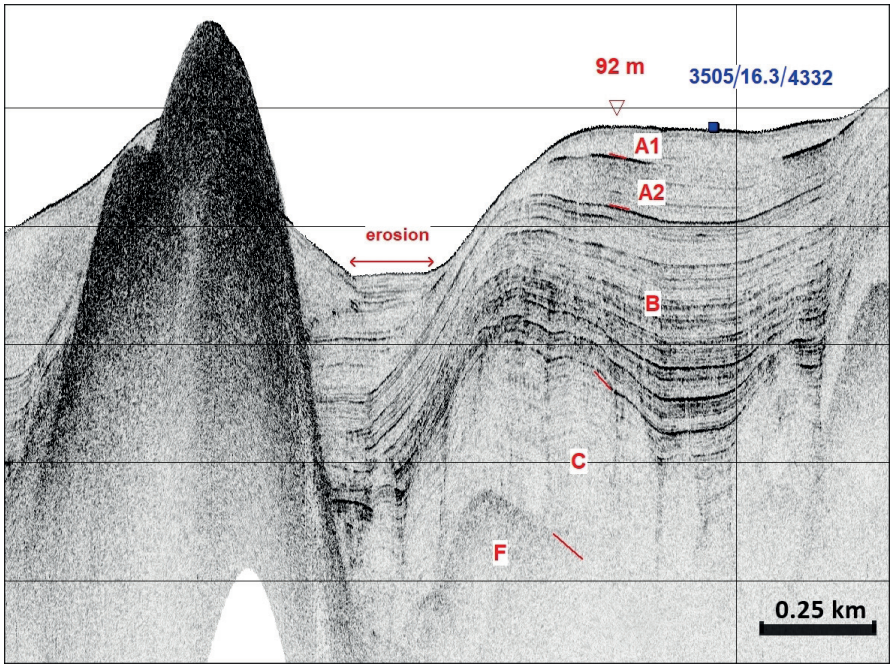

Fig. 5. Maximum section of the sedimentary cover (92 m) along profile 707_2 in the area of station 3 505 (16.3 kg/m^2, depth 4 332 m) (Dreiseitl, 2018).

In several places of the profile, bottom sediments are missing and basement rocks in the form of cliffs and/or volcanic edifices emerge. Near the outcrops, the thickness of bottom sediments is considerably reduced.

Physical and strength properties of bottom sediments in H22 exploration block

Determination of the physical and strength properties of bottom sediments was carried out at 50 sampling stations collected in expeditions until 2014. The sampling depth was determined by the possibility of taking samples of undisturbed composition and not exceeding 0.44 m.

Determination of the moisture and soil density was carried out on 125 samples. The test of penetration resistance, vane shear strength and the residual strength of sediment was performed on 98 samples. The following parameters were calculated: parameters of dry unit weight, porosity, porosity factor and bulk density, and the over-consolidation ratio.

Figure 6 presents the water content and density values of the two observed types of bottom sediments, evaluated in an on-board laboratory. The difference between the siliceous varieties of bottom sediments (blue points) and non-siliceous red pelagic clays (red points) can be observed, confirming their different engineering-geological properties. The bottom sediment samples, selected for engineering and geological studies, were analysed in two ways (Dreiseitl, 2018):

- according to the type of bottom sediments,
- according to the depth of sampling intervals.

The types of bottom sediment (Dreiseitl, 2018):

Siliceous clay silt with an increased content of diatoms (SILETM), with amorphous silica content exceeding 20 %, analysed on samples drawn from depth 2 to 30 cm. In the case of a GAL sample (geochemically active layer, 0–7 cm), which is of semi-liquid state, determination of the strength properties was impossible.

Siliceous clay (SIL) with amorphous silica ranging from 10–20 %, is the most common sediment type in the H22 exploration block. They are found at the depths from 2 to 30 cm.

Slightly siliceous clay (SLSIL) with amorphous silica ranging from 5–10 %, can be found in the depths ranging from 10 to 30 cm.

Red pelagic clay (RPC) is charac-

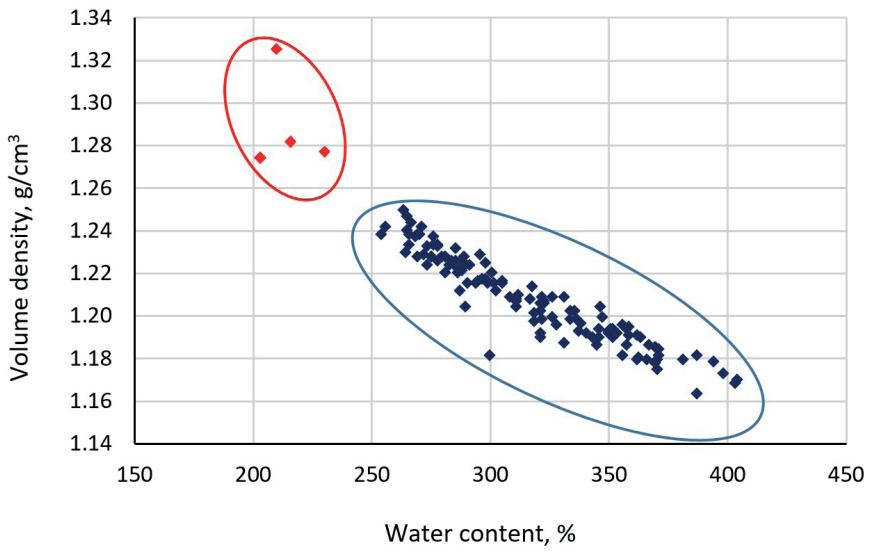

Fig. 6. Distribution of siliceous (blue area) and non-siliceous (red area) types of the sediments, according to soil volume density and water content (Dreiseitl, 2018).

terized by an amorphous silica content less than 5 %. They were found in depth interval 8 to 44 cm.

The mean values for the physical and strength properties of different types of bottom sediments in the H22 exploration block are given in Tab. 2

The depth intervals analysed:

0–7 cm – geochemically active layer (GAL),

8–20 cm – the predominant sampling interval was 10–15 cm,

25–32 cm – predominant sampling interval was 25–30 cm,

> 32 cm.

The mean values for the physical and strength properties according to the depth of sampling intervals in the H22 exploration block are given in Tab. 3.

Variability of the water content and the sediment density, together with the depth, is shown in Fig. 7 (the deeper the sediment is deposited, the denser it is – a result of squeezing sea water from the pore space). The highest water content was measured in the GAL sediments (range 0–7 cm), which are in direct contact with seawater and, accordingly, these precipitates are characterized by low density.

Based on the strength analysis of the particular bottom sediments in the exploration block H22 at the depth interval of 8–20 cm (prevailing sampling interval of 10–15 cm) a map of strength properties in a scale 1 : 400,000 was prepared. An interval of 8–20 cm includes the first underlying layer at all stations. The second underlying layer, usually at the 25–30 cm interval, is not disclosed at all stations. The average strength of bottom sediments of

Tab. 2

The mean values for the physical and strength properties of different types of bottom sediments in the H22 exploration block (Dreiseitl, 2018).

Sediment type	Number of tests	Water content [%]	Density [g/cm^3]	Dry unit weight [g/cm^3]	Porosity [%]	Porosity factor	Bulk density [g/cm^3]	Number of tests	Penetrtation resistance [kPa]	Shear strength [kPa]	Residual strength [kPa]	Overconsolidation ratio
SIL (ETM)	19	347	1.19	0.27	90	9.24	2.73	15	2.0	2.7	1.4	2.2
SIL	86	319	1.21	0.29	89	8.55	2.75	64	4.1	4.2	1.7	2.5
SLSIL	15	274	1.23	0.33	88	7.40	2.77	16	7.9	7.0	2.5	2.8
RPC	5	226	1.28	0.39	86	6.40	2.90	3	22.3	12.9	4.0	3.3

Tab. 3

The mean values of the physical and strength properties of bottom sediments according to sampling depths in the H22 exploration block (Dreiseitl, 2018).

Sampling interval [cm]	Number of tests	Water content [%]	Density [g/cm^3]	Dry unit weight [g/cm^3]	Porosity [%]	Porosity factor	Bulk density [g/cm^3]	Number of tests	Penetrtation resistance [kPa]	Shear strength [kPa]	Residual strength [kPa]	Overconsolidation ratio
0–7	29	359	1.19	0.26	91	9.71	2.77	0	–	–	–	–
8–20	47	310	1.21	0.30	89	8.26	2.73	50	3.9	4.0	1.7	2.4
25–32	47	292	1.22	0.31	89	7.88	2.77	48	6.1	5.3	2.0	2.7
> 32	2	243	1.26	0.37	87	6.65	2.80	0	–	–	–	–

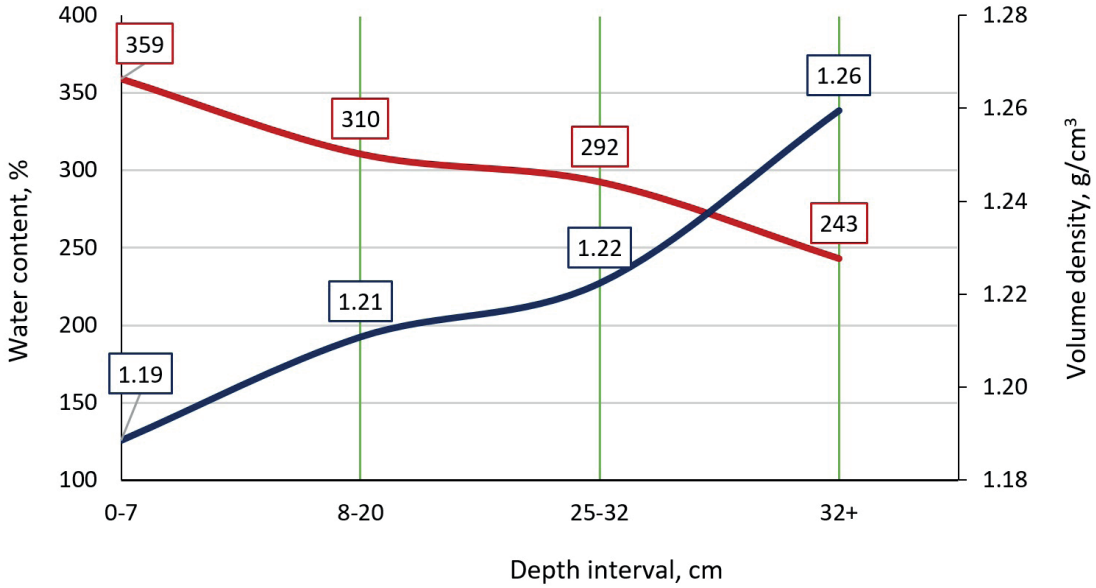

Fig. 7. Vertical variability of water content (red line) and density (blue line) of the bottom sediments in the H22 exploration block (Dreiseitl, 2018).

the second layer (5.3 kPa), exceeds the average strength of the first layer (4.0 kPa).

Geochemical properties of bottom sediments in H22 exploration block

The active pH reaction and the redox potential Eh are the main geochemical indicators of bottom sediments, which can be used to study the processes of oxidation and/or hydration. The measurement results (191 pairs) for the sampling intervals shown in Tab. 4, belong to the bottom sediments of GAL and all three known siliceous varieties: siliceous clayey silt, slightly siliceous clayey silt, and ethmodiscus silt. Both in the values of the active reaction of the medium and the redox potential of bottom sediments in relation to the depths of sampling, as well as to the depths of the ocean (Fig. 8), no anomalies were observed. Values of Eh < 400 mV were generally not observed in the study area, except for 4 values of Eh in the interval 300–400 mV (red points in Fig. 8). The range of pH variability is 7.10–7.80, which characterizes the environment from weakly alkaline (7.50–7.80) to neutral (7.00–7.50). The range of Eh variability does not exceed (without taking into account 4 extreme values) 160 mV.

Red pelagic clays were identified at 6 sampling stations, where 7 data pairs were obtained. The range of pH variability is 7.33–7.59, which characterizes the environment as neutral. All Eh values are > 400 mV and the range of variability reaches 190 mV (Dreiseitl, 2018).

Tab. 4

Active reaction and redox potential of siliceous clayey silts of H22 exploration block (Med – medium value, Max – maximal value, Min – minimal value) (Dreiseitl, 2018).

Sampling depth [cm]	Number of asurement pairs	pH			Eh [mV]		
		Med	Max	Min	Med	Max	Min
0–3 (GAL)	49	7.48	7.60	7.21	473	553	402
3–5 (GAL)	14	7.44	7.56	7.23	481	551	437
5–10 (GAL)	10	7.42	7.51	7.30	470	501	420
10–15	50	7.42	7.62	7.10	484	565	415
25–30	47	7.45	7.80	7.12	468	553	403
> 30	21	7.37	7.72	7.24	484	517	422
	191						

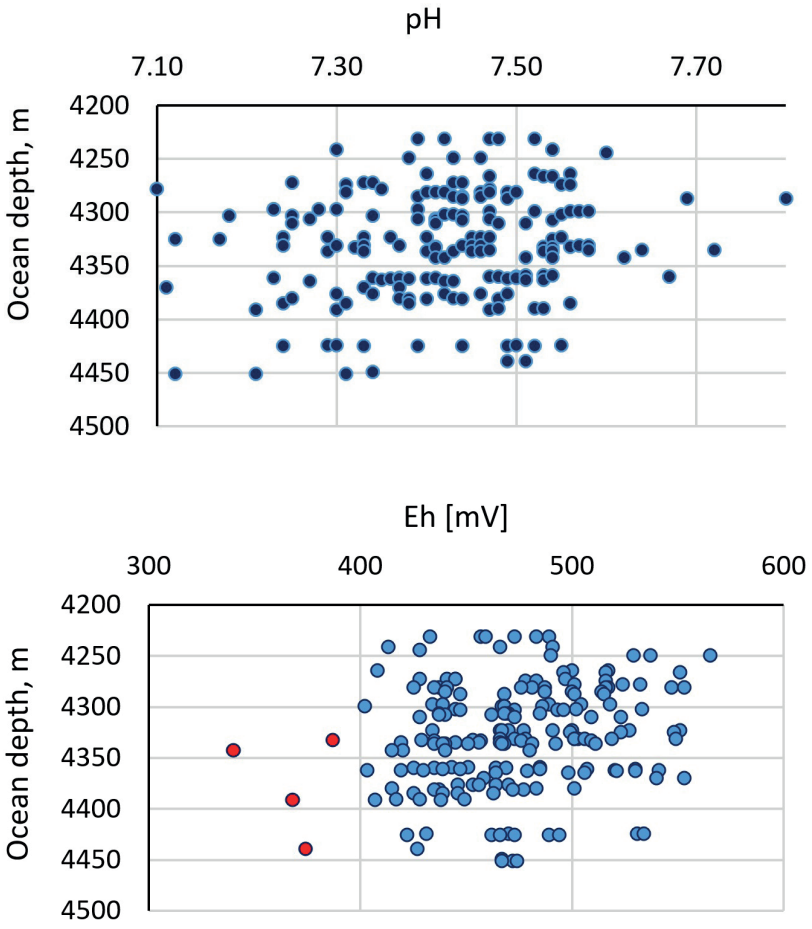

Fig. 8. Distribution of pH and Eh values of bottom sediments in geologically active layer (GAL) over the ocean depth in the H22 exploration block (Dreiseitl, 2018).

Selected metal contents of bottom sediments in H22 exploration block

Determination of 9 metal contents (Fe, Mn, Ni, Cu, Co, Zn, Pb, Cd and As) was carried out in the on-board laboratory at 65 samples, representing 23 stations (IOM-2014 cruise). Samples were taken in three depth intervals (0–5, 10–15 and 25 + cm). In siliceous sediments, manganese (5 582 to 2 020 ppm) and nickel (228 to 112 ppm) content decreases with depth, iron content (4.57 to 4.90 %) increases with depth. Regularities were not found for the rest of metals (Cu 337 to 466 ppm, Co 47 to 65 ppm, Zn 140 to 146 ppm). The higher content of all elements is associated with the presence of micronodules in the sediment, as well as ore material near the crusts, which are often concentrated in the top layer of red pelagic clays (Dreiseitl, 2018).

More detailed analyses of chemical composition of bottom sediments were carried out in stationary (land) laboratory (Tab. 5). Samples from the same intervals of depth were used (0–5, 10–15 and 25+ cm). The total average content of rare earth elements in sediments (REE – 14 elements from La to Lu, without Sc and Y) is 277 mg/kg, which is approximately 2 times less than that in nodules. Red pelagic clays represent the sediments with the most abundance of metals (Dreiseitl, 2018).

In bottom sediments (without distinguishing individual sediment types), basic metals have an increased content in interval 0–5 cm, due to the presence of micronodules, as well as in interval more than 25 cm, which signals the proximity of layer of red pelagic clays and the presence of ore crusts on its top. Interval 10–15 cm is influenced by recent sedimentation, which is manifested by an increased content of amorphous silica and decreased content of metals. In the red pelagic clays, there is also an increased content of rare earth elements (in some samples reaching values over 300 ppm).

Tab. 5

Average values of selected metal contents of bottom sediments by sampling depths (SIL = siliceous sediments, value in brackets = number of analysed samples) (Dreiseitl, 2018, modified).

Sediment type / Sampling interval [cm]	%		ppm						
	Fe	Mn	Ni	Cu	Co	Zn	Pb	Cd	As
SIL [0–5]	4.50 (10)	0.46 (10)	159 (11)	349 (11)	63 (11)	126 (11)	18 (11)	0.22 (11)	7.17 (11)
SIL [10–15]	4.58 (10)	0.32 (10)	109 (11)	299 (11)	52 (11)	121 (11)	19 (11)	0.12 (11)	5.76 (11)
SIL [25–30]	4.75 (11)	0.57 (11)	198 (12)	476 (12)	96 (12)	136 (12)	23 (12)	0.23 (12)	6.91 (12)
Red pelagic clays [11–44]	5.63 (3)	2.05 (3)	508 (4)	944 (4)	224 (4)	187 (4)	31 (4)	0.60 (4)	9.02 (4)

Selected metal contents in sediments of H22_NE exploitation block

In total, 60 samples were analysed. The mean Fe content (4.42 + 0.90 %) is higher than those of Mn (0.40 + 0.33 %). The mean Mn/Fe ratio is 0.08. The Mn and Fe contents increased with depth, the increase in some cases being related to the formation of diagenetic micronodules. Among metals other than Mn and Fe, dominant were Cu and Ni. The mean Cu and Ni contents were 388.3 + 101.5 ppm and 141.0 + 73.4 ppm, respectively. The content of Cu, Ni, Co, Zn and Pb were gradually increasing with depth. The As and Cd contents were low, with means of 8.4 + 3.0 ppm and 0.14 + 0.13 ppm, respectively. The mean ∑REE content was 285.8 + 127.9 ppm, with LREEs dominating over HREE. Among the REEs, the highest contents were shown by Y, Ce, Nd and La. Like those of other metals, the REE contents were gradually increasing with depth, the increase being particularly pronounced (to more than 400–500 ppm) below 40–50 cm. In contrast, the ∑REE content in GAL and below was fairly uniform (Maciąg et al., 2021).

The gradual increase in the contents of all metals, including REEs, with depth (Fig. 9) has to be regarded as associated with diagenetic processes which are particularly intensive below 30–40 cm in the sediment (Maciąg and Zawadzki, 2019; Zawadzki et al., 2020).

Grain size analysis of sediments in H22_NE exploitation block

The sediment in most samples was mostly slightly plastic, slightly to moderately sticky, slightly hard, and mottled. Few samples showed the sediment to be non-plastic or soft as well as gelatinous or brittle. Traces of bioturbation were found in 58 out of the 90 samples examined. An increased amount of micronodules, nodule remains and some unidentifiable biogenic remnants or intraclasts were observed in 15 samples.

None of the samples showed the presence of $CaCO_3$, as tested with 10 % HCl. The absence of carbonates in the form of calcite or aragonite was additionally confirmed by the XRD analysis.

The sediments examined represented sandy silts, clayey silts and silts. Several samples were inhomogeneous enough to be classified as sand-silt-clay (Fig. 10). The sediments examined were generally very poorly and poorly sorted. The low amounts of very fine gravel and very coarse

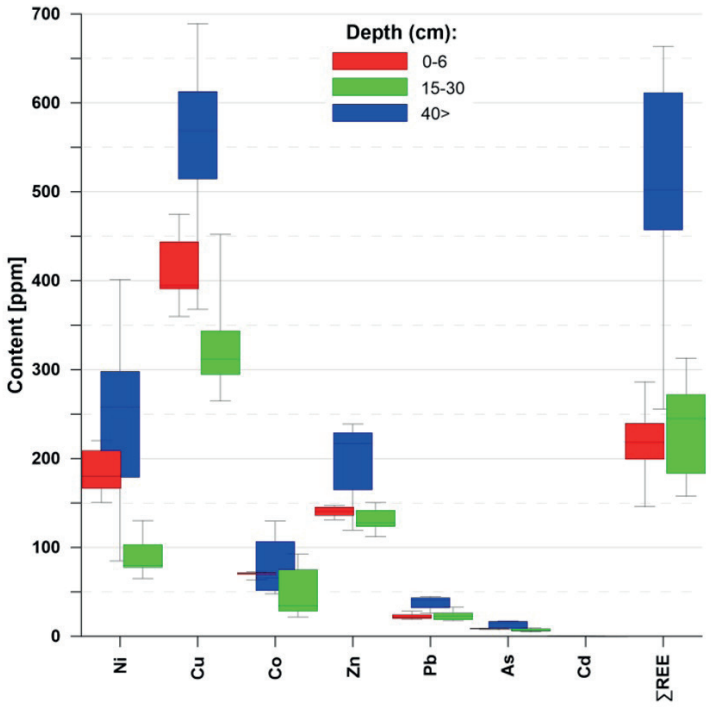

Fig. 9. Box-and-whiskers plots of depth-related variability in contents of selected metals. Whiskers indicate the minimum and maximum values; boxes show the lower (25 %) and upper (75 %) quartile of the data (Maciąg et al., 2020).

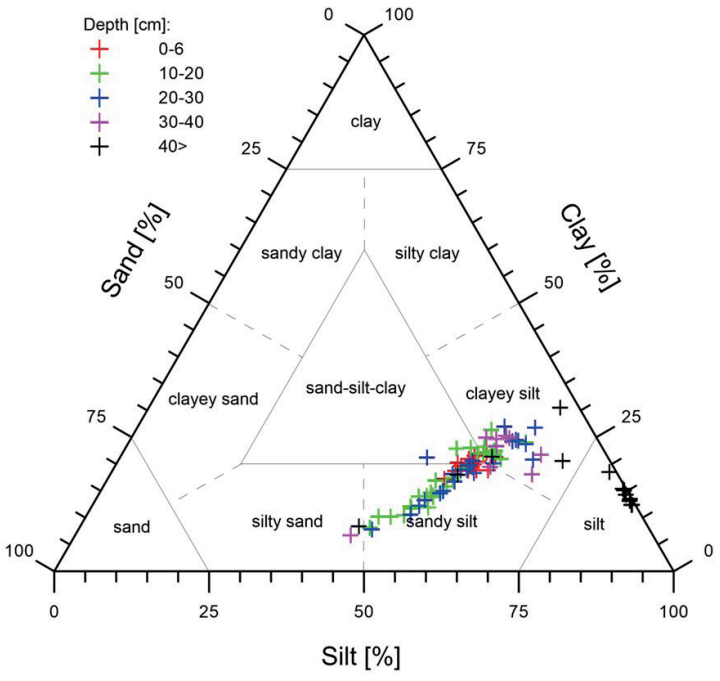

Fig. 10. The Shepard (1954) ternary diagram indicating the dominance of sandy silts, clayey silts, silts and a mixed group of sand-silt-clay (Maciąg et al., 2020)

sand subfractions found can be related to the presence of polymetallic nodule fragments or micronodules. The clay fraction content varied from 6.71 to 30.55 %, increasing with depth in the sediment.

The mean grain size varies from 6.99 to 47.00 μm (4.41–7.16 Φ), with a mean of 18.48 μm + 8.08 μm (5.88 Φ). Sorting varied from 2.23 to 6.63 μm, with a mean of 4.05 μm. Skewness varied from –0.43 to 0.20 (Maciąg et al., 2020).

Amorphous silica content in sediments of H22_NE exploitation block

The UV-VIS analyses showed elevated contents of biogenic silica (amorphous siliceous phase represented by opal-A), which was also indicated by the XRD analyses (Maciąg et al., 2020). The biogenic SiO_2 contents were found to vary within 9.28–39.04 % (mean of 22.51 + 6.02 %). These values are about 12 to 15 % lower than the XRD data; however, they do not include other amorphous mineral phases such as volcanic glass or allophanes (Maciąg et al., 2011). Additionally, the XRD analyses of the amorphous phase carried a higher potential error, related mainly to the underestimation of the diffractogram background (Kowalska, 2014).

The amorphous silica content was observed to decrease with increasing depth in the sediment, the clay mineral contents increasing with depth (Fig. 11). Particularly distinct was the increase in the smectite content with depth in the sediment. The illite content increased only within 15–30 (35) cm, usually decreasing below that level. All those changes are associated with the chemical decomposition of biosilica or volcanic glass and their transformation to new mineral phases, such as smectite (Zawadzki et al., 2020).

Total carbon (TC), total nitrogen (TN), total sulphur (TS), total organic carbon (TOC), and total inorganic carbon (TIC) contents in sediments of H22_NE exploitation block

As shown by the analyses of biogenic components, the total carbon (TC) contents were low (0.101–0.680 %; mean of 0.352 + 0.146 %). The carbon species were dominated by organic carbon (TOC), the contents of which were observed to vary within 0.068–0.582 % (mean of 0.332 + 0.170 %). The total inorganic carbon (TIC) contents were extremely low (< 0.147 %), as additionally confirmed by the lack of sediment reaction with HCl (see above) and no trace of carbonate minerals revealed by XRD. The total nitrogen (TN) contents were very low (0.016–0.118 %; mean of 0.073 + 0.026 %). Compared to TN, the contents of total sulphur (TS) and total phosphorus (TP) contents were higher (0.216–0.956 %; mean of 0.503 + 0.15 % and 0.066–0.435 %; mean of 0.136 + 0.088 %, respectively).

The TC and TOC contents were observed to gradually decrease with depth; a similar pattern was seen in the TN and TS contents. An opposite behaviour was detected in the TP contents which were increasing with depth (Fig. 11). The decreasing contents of most biogenic components with depth is typical and associated with oxygen consumption during denitrification and desulphurization (Volz et al., 2018). The increase in the phosphorus content below 40 cm should be regarded as strongly associated with increasing contents of ∑REE (Maciąg et al., 2020).

XRD analyses

The sediment samples analysed showed a relatively low variability of their mineral components (Maciąg et al., 2020). The bulk X-ray diffraction analysis revealed domination of two major component groups: (i) amor-

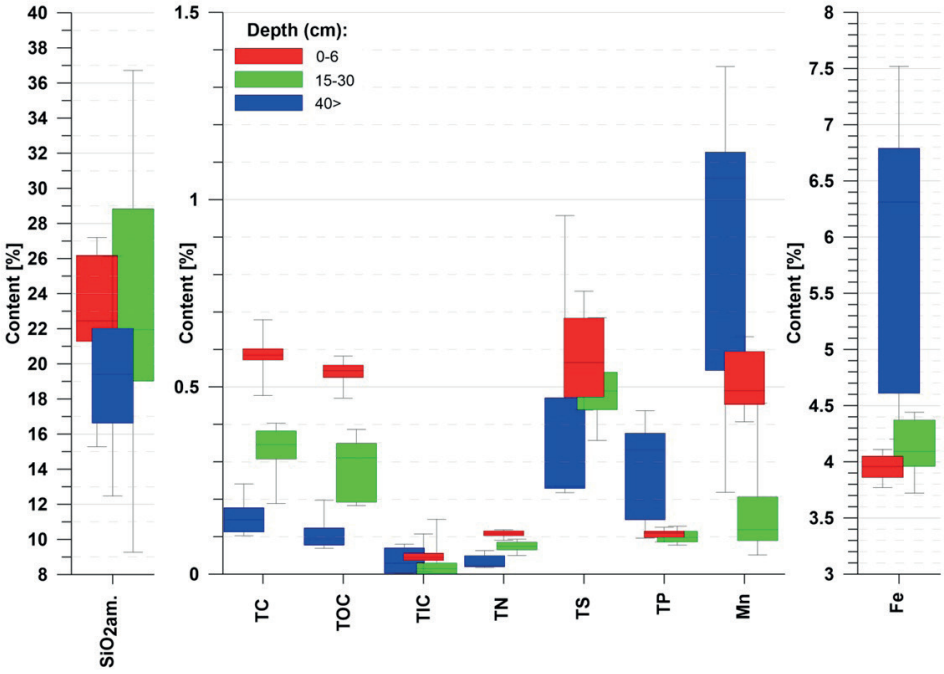

Fig. 11. Box-and-whiskers plots of depth-related variability in contents of biogenic components (including amorphous biosilica) as well as Mn and Fe. Whiskers indicate the minimum and maximum values; boxes show the lower (25 %) and upper (75 %) quartile of the data (Maciąg et al., 2020).

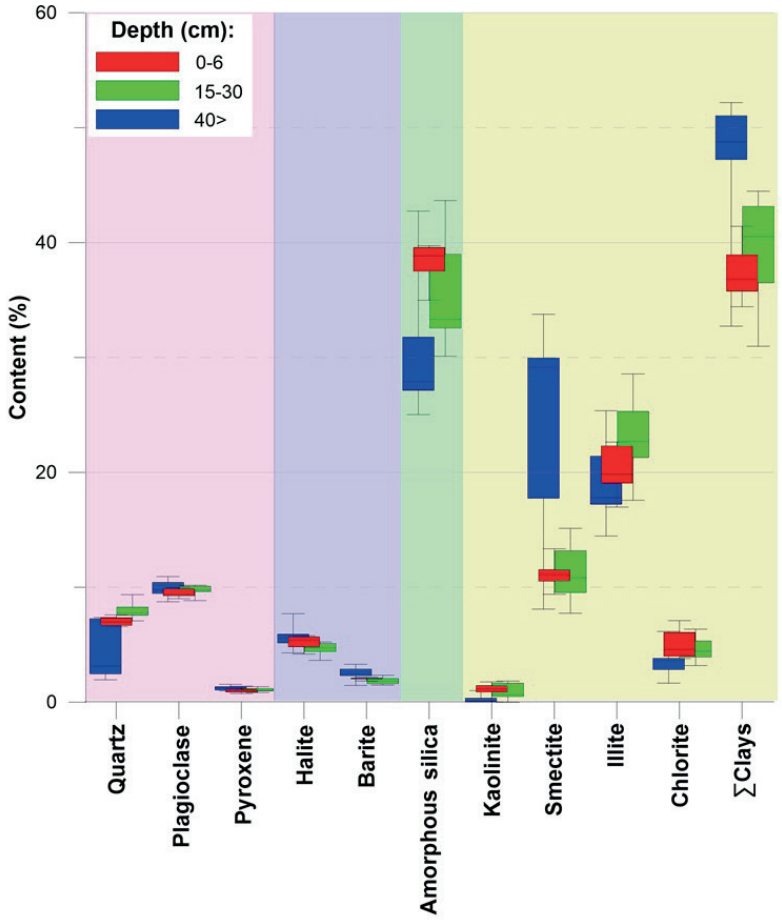

Fig. 12. Box-and-whiskers plots showing the depth-related variability in contents of the minerals identified. Whiskers indicate the minimum and maximum values; the boxes show the lower (25 %) and upper (75 %) quartile of the data (Maciąg et al., 2020).

phous biogenic silica represented by opal-A, and (ii) clay minerals. Their contents varied within 25.01–47.67 % and 25.86–52.16 %, respectively. The mean contents of amorphous silica and clay minerals were 35.32 % + 5.56 % and 40.06 + 6.26 %, respectively. The clay minerals were dominated by illite (I) and smectite (S), with mean contents of 20.67 % and 14.32 %, respectively. The mean I/S ratio was 1.75 + 0.63. The chlorite content varied within 1.64–7.10 % (mean of 4.32 % + 1.13 %). Kaolinite occurred in trace amounts only, up to 1.89 %, and usually below 1 % (Fig. 12). The allogenic detrital components were dominated by plagioclases and quartz, with ranges of 8.60 to 11.05 % and 1.93–9.41 %, respectively and the mean contents of 9.71 % + 0.55 % and 6.67 % + 1.92 %, respectively. In addition, pyroxenes were detected, usually in trace amounts (up to 1.54 %, and usually below 1 %). Diagenetic minerals featured halite (3.15–7.68 %; mean of 5.08 % + 0.80 %) and barite (1.44–3.28 %; mean of 2.05 + 0.41 %).

SEM/EDX analyses

The scanning electron microscopy (SEM) photographs were taken and energy-dispersive X-ray (EDX) micro-geochemical analyses were conducted, 103 photographs were taken and 137 EDX analyses were performed. A total of 45 slurried samples were selected based on a macroscopic description, grain size analysis, bulk geochemistry and XRD results (Maciąg, 2021).

The sediments analysed showed the presence of a large variety of mineral and biogenic components as well as various debris. Generally, the contents of those components varied little in all the profiles analysed, the variability being partially related to burial-associated degradation and diagenesis of sediments.

Biogenic components were dominated by siliceous radiolarian skeletons, with lower amounts of sponge spicules and a minor presence of diatom frustules. The amount of siliceous bioclasts usually decreased with depth in the sediment; morphological preservation of the bioclasts declined with depth in the sediment, and contrasted with the best-preserved structures found in the GAL. The siliceous bioclasts, particularly radiolarians, showed traces of corrosion and alteration, evidenced by overgrowths of initial clay minerals.

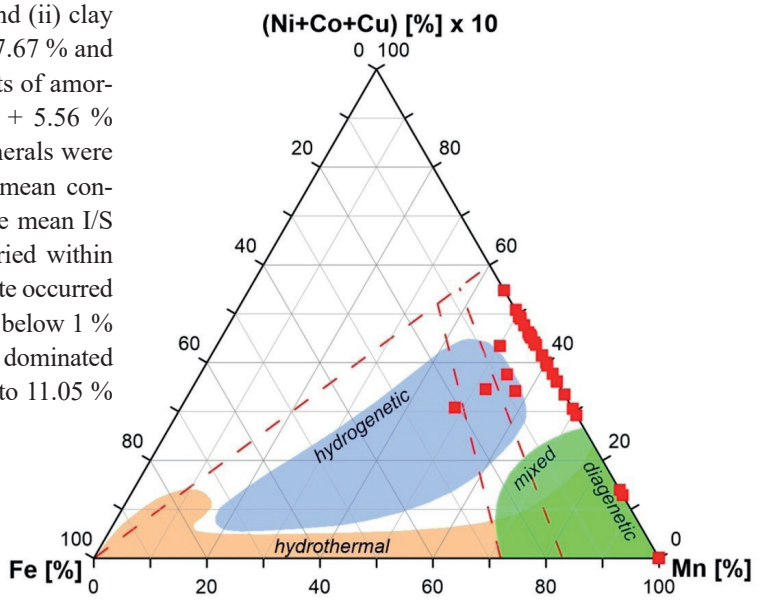

Fig. 13. Classification of the micronodules analyzed (N = 35) after Bonatti et al. (1972), with modifications (Maciąg, 2021).

Increased contents of bioapatite were observed below the depths of 40–50 cm in the sediment (cores 3632T and 3633T), indicating a relatively low substitution with alkali and alkaline metals, Mn-Fe impurities or Cl. One grain showed the presence of more than 5 % ΣREE. Some apatites were of magmatic rather biogenic origin, as evidenced by increased F contents.

A few samples from below 40 cm in the core showed increased contents of authigenic barite. Additionally, cores 3632T and 3633T showed the presence of zeolites, particularly within 60–110 cm of core depth. Interestingly, although the zeolites indicated Ba impurities, no barite was identified in those samples with increased zeolite contents.

The Mn-micronodules analysed were of a typical diagenetic-hydrogenetic origin (Fe contents very low or below EDX detection limits) and showed increased contents of Ni and Cu (4–8 %); in a few cases, traces of Co and Zn were revealed (Fig. 13). Organic burrows showed coatings enriched with Mn-oxyhydroxides, suggesting the processes of bio-irrigation and bio-oxidation.

The allogenic debris components were represented by minor plagioclases (anorthite-labradorite series) as well as by altered amphiboles and pyroxenes. The absence of detrital quartz grains suggests their presence within the fine pelitic fraction. In a few cases, volcanic glass was identified (e.g. among zeolites identified in cores 3632T and 3633T) (Maciąg, 2021).

Polymetallic nodules

Mineral composition

The detailed mineralogical and microgeochemical characteristics of polymetallic nodules collected during IOM-2014 and IOM-2019 expeditions from IOM exploration area (H22_NE exploitable block) were studied (Skowronek et al., 2021). The data were applied for the delimitation of nodule growth generations and estimation of the growth ratios (back-stripping using the Co-chronometer method). The applied methods included bulk X-ray powder diffraction (XRD) and electron probe microanalysis (EPMA), providing information about Mn-Fe minerals and clays composing nodules, as well as the geochemical zonation of the growth generations.

The analysed samples are generally dominated by todorokite/buserite, with a lesser amount of birnessite and traces of vernadite. Additionally, the samples indicated the presence of Fe-rich clay minerals (potentially nontronite and Fe-smectite) and mixtures of quartz, barite, zeolites (potentially Na-phillipsite), apatite, and barite (Tab. 6).

The analysed nodules were mostly diagenetic (Mn/Fe > 5), with less influence on the hydrogenous processes, dominated by the presence of 10-Å phyllomanganates represented by todorokite/buserite, additionally mixed with birnessite and vernadite. The specific lithotype (intranodulith), being an integral part of polymetallic nodules, de-

Tab. 6

Mineral compositions of the selected polymetallic nodule samples from the H22 exploration block, as determined by XRD. The amount of minerals is shown semi-quantitatively based on the results of the peak comparisons and integration: ++++ dominating < 50 %, +++ 50–30 %, ++ 30–10 %, + 10–5 %, and (+) traces < 5 % (Skowronek et al., 2021).

Sample	Type	Todorokite/ Busserite	Birnessite	Vernadite	Clays	Barite	Apatite	Zeolites	Quartz
3529	D	+++	++	(+)	+	(+)	++	+	(+)
3535	D	+++	+++	(+)	+	(+)	+	+	(+)
3537A	D-HD	+++	+	(+)	++	(+)	(+)	++	+
3537B	D-HD	+++	++	(+)	++	(+)	+	–	+
3542	H	+++	++	(+)	++	(+)	+	++	(+)
3602	D	++++	++	(+)	–	(+)	(+)	+	(+)
3603	D	+++	++	(+)	++	(+)	(+)	+	+
3604	D	++++	++	(+)	+	(+)	(+)	+	(+)
3605	D	+++	+++	(+)	++	+	–	–	–
3613	HD	+++	++	(+)	++	(+)	++	+	(+)
3614	H-HD	++++	++	(+)	+	(+)	–	++	(+)
3615	H-HD	++	++	(+)	++	(+)	–	+++	(+)

veloped as a result of the secondary diagenetic processes of lithification and the cementation of Fe-rich clays (potentially nontronite and Fe-rich smectite), barite, zeolites (Na-phillipsite), bioapatite, biogenic remnants, and detrital material, occurs in holes, microcaverns, and open fractures in between ore colloforms. The contents of å(Ni, Cu, and Co) varied from 1.54 to 3.06 wt %. Several remnants of siliceous microorganisms (radiolarians and diatoms) were found to form pseudomorphs. The applied Co-chronometer method indicated that the nodules' age is mainly Middle Pliocene to Middle Pleistocene, and the growth rates are typical of diagenetic and mixed hydrogenetic-diagenetic (HD) processes. Additionally, few nodules showed suboxic conditions of nucleation. Growth processes in the eastern part of the CCZ deposit might have been induced with the Plio-Pleistocene changes in the paleooceanographic conditions related to the deglaciation of the Northern Hemisphere.

The analysed polymetallic nodules consist of a core concentrically overgrown by laminae (microlayers) and areas of lithified detrital materials. The core, the laminae, and the detrital material were considered separately. The core is composed of either fragments of ancient nodules (here, Mn-Fe laminae are clearly visible) or fragments of rocks (an absence of laminae). The growth structures (laminae) overgrowing the core developed as colloforms composed of precipitated Mn-rich oxyhydroxides, mainly Ni–Cu-rich todorokite/10-Å phyllomanganates (buserite) and birnessite (Fig. 5a–d). The number of laminae composed of vernadite is relatively low (Fig. 14).

The results of the spot EPMA evidenced the nonuniform distribution of the metals in the nodules. Several of the measurement points were characterized by high concentrations of Mn in relation to Fe and were assigned to the traditionally defined diagenetic morphotype (Mn/Fe ratio > 5). The measurements typical for hydrogenetic or mixed (hydrogenetic-diagenetic-biogenous) morphotypes, i.e., depleted in Mn in comparison to the diagenetic morphotype, were less frequent (Fig. 15). The elevated contents of Fe (plots near the Fe edge) measured for nearly 30 points in all the analysed nodules were associated with the intercalation of the clay minerals and other components of detrital origin (enriched with Si, Al, or alkali-alkaline metals).

In general, regardless of the internal differentiation of the nodules, the mean Mn and Fe contents varied from 19.6 to 38.9 wt % and from 3.2 to 8.3 wt %, respectively. The mean Mn/Fe ratio was 5.37. Among the other economic metals, Ni and Cu dominated, with their mean contents varying from 0.60 to 1.52 wt % and 0.64 to 1.42 wt %, respectively. The mean EPMA contents of Ni and Cu were 1.15 and 1.08 wt %, respectively. The Co concentration varied from 0.06 to 0.31 wt %, averaging 0.20 wt %. The hydrogenetic and mixed hydrogenetic-diagenetic nodules showed lower contents of å(Cu, Ni, and Co) compared to the diagenetic nodules, with concentrations varying from 1.54 to 2.07 wt %. Additionally, low contents of Zn were identified (mean = 0.14 wt %, varying from 0.07 to 0.19 wt %), as well as Pb, As, Cr, and V (Skowronek et al., 2021).

Polymetallic nodules collected in the IOM licence area (H22-NE expoitation block) showed complex internal textures reflecting multistage nucleation affected by potential changes in the paleoproductivity and surface temperatures

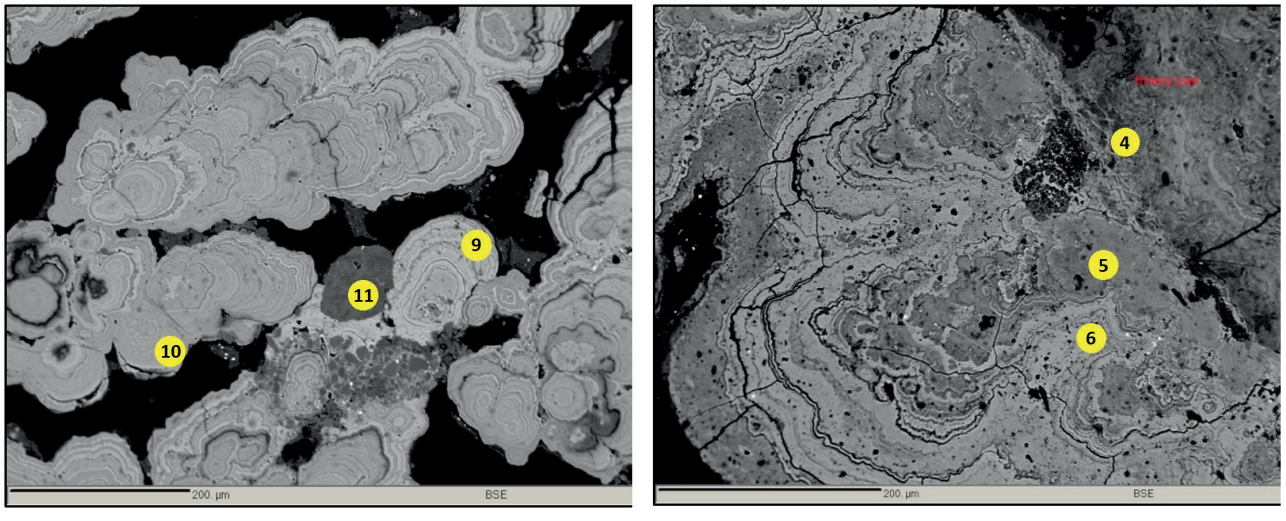

(a) **(b)**

Fig. 14. Representative EPMA BSE images of the analysed polymetallic nodules. Sample 3642: (a) massive bright and well-developed colloforms composed of pure Mn oxyhydroxides enriched with Ni and Cu (9,10); no. 11 is an intraclast of Fe-rich clay minerals. Sample 3602: (b) typical Mn-rich diagenetic colloforms enriched with metals (5,6) and bordering a zone of veinlets and Fe-rich clay aggregates (4) (Skowronek et al., 2021).

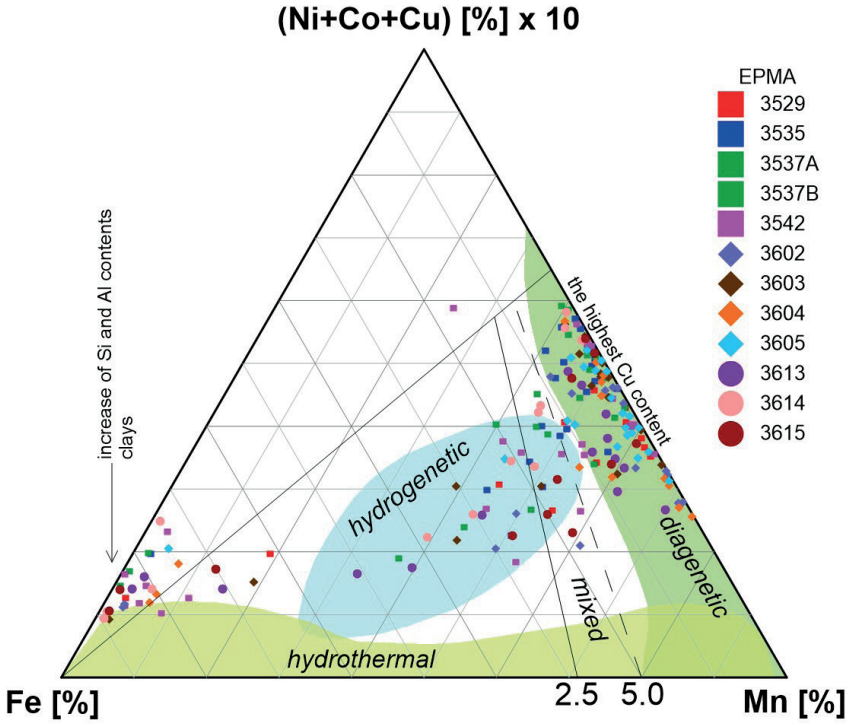

Fig. 15. Location of the EPMA spot data at the Fe–Mn-10 [å(Ni, Co, and Cu)] ternary plot; 2.5–5.0 = Mn/Fe ratio (reference [63] with further modifications). Coloring identifying major genetic types of analysed colloforms (Skowronek et al., 2021).

occurring during the Late Pliocene-to-Middle Pleistocene (Plio-Pleistocene) postglacial transition. Most of the analysed samples showed distinctive diagenetic features evidenced by relatively high growth rates (> 5 mm/Myr), increased Ni + Cu + Co contents (> 4 wt %), and admixtures of Fe-rich clays or barite.

The polymetallic nodules located in the nearest vicinity to underwater volcanic-shaped areas usually showed higher inputs of the hydrogenic components (slow growth rates, increased amount of Fe, and the presence of vernadite) compared to the nodules collected in relatively flat, streaked, and meridian-oriented blocks of the seafloor.

Intranodulith was proposed as a term describing the specific lithotype that is the integral part of polymetallic nodules, which developed as a result of the secondary diagenetic processes of lithification and cementation of

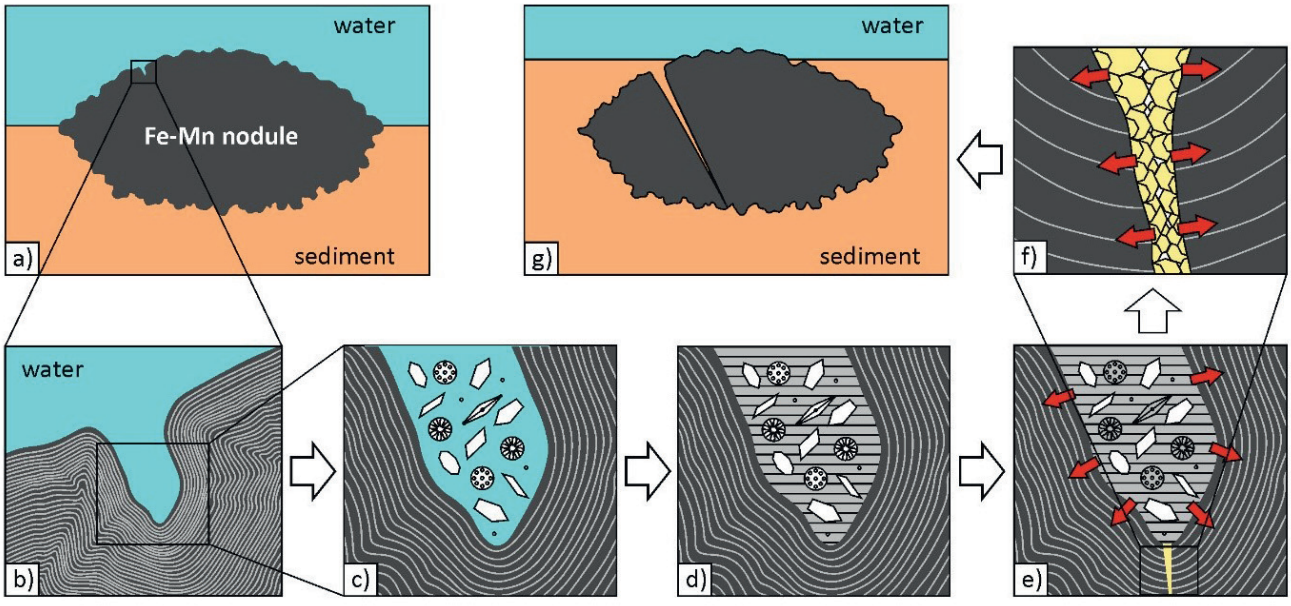

Fig. 16. Simplified scheme of nodule cracking due to cement growth: (a–g) the steps of the cracking process from a solid (a) to a broken nodule (g). Nodule crack caused by internal tension in the vein created by crystal growth inside the intranodulith. Red arrows indicate internal tension forces (Skowronek et al., 2021).

trapped detrital materials within holes, microcaverns, or open fractures in between ore colloforms.

A hypothesis of nodule cracking on the seafloor being caused by internal tension in the vein created by crystal growth was proposed (Fig. 16). An increase in the volume during the diagenetic lithification of the sediments trapped in cavities between colloforms (intranodulith) might have been responsible for the initial impulse that ultimately led to cracks of the Mn-Fe nodules. The further growth of the cement crystals within the initial fissure led to their additional extension, which could have ultimately caused the breakage of the nodules directly at the seafloor, being evidenced, e.g., in seabed photos or photo profiles. This secondary diagenetic process can cause the disintegration of the whole nodule without the influence of any external factors – the nodule disintegrates "by itself" (Skowronek et al., 2021).

Chemical composition

The reference sample of the polymetallic nodules was prepared. Homogeneity was determined by XRF analysis taken from different places of the homogenized material in the mixing container. The mixing process was repeatedly formed until the standard deviations for Mn, Fe, Si, Al, Ni, Cu, Mg and Cl under 0.23, 0.06, 0.1, 0.04, 0.03, 0.03, 0.15 and 0.06, respectively were achieved. In total, 50 g of the homogenized reference material was prepared (Vu et al., 2020).

The reference contains 95 % of the particles with the particle size under 45 μm and its humidity is in the range from 1.6 to 2.1 %. The average chemical composition of the reference for the main metals is listed in Tab. 7. The chemical composition of the main metals was calculated from the results provided by 5 laboratories. The obtained results show that laboratories using the wet method (FAAS, ICP-MS, ICP-AES) provided almost identical results for analysis of the main metals. Spectroscopic methods (XRS, XRF) provide either higher or lower metal content for Mn, Ni and Cu.

Tab. 7

Average content of main metals in the reference material [wt %] (Vu et al., 2020).

	Mn	Fe	Ni	Cu	Co	Mo	Zn	Pb	P
Average	30.817	5.385	1.313	1.305	0.165	0.080	0.153	0.026	0.150
Min	29.660	4.930	1.030	1.060	0.130	0.060	0.130	0.022	0.136
Max	32.600	5.790	1.510	1.550	0.200	0.130	0.170	0.029	0.162
St. Dev.	1.048	0.292	0.161	0.160	0.023	0.034	0.014	0.003	0.011
RSD [%]	0.035	0.054	0.122	0.123	0.137	0.421	0.089	0.129	0.072

Main metals of H22_NE exploitable block were studied by AAS and XRF methods. Comparison of the results of both methods is shown in Tab. 8.

Tab. 8

The chemical composition of nodules (base metals) in H22_NE exploitable block, determined by the AAS and XRF methods (Vu et al., 2020).

n = 20	Mn [%]	Fe [%]	Ni [%]	Cu [%]	Co [%]	Zn [%]	Mo [%]	Pb [%]	Mn/ Fe ratio	ΣNi, Cu, Co [%]
AAS	26.99	5.78	1.27	1.20	0.18	0.15	0.05	0.03	4.85	2.65
XRF	30.10	6.07	1.33	1.27	0.20	0.15	0.07	0.03	5.14	2.81

In H22_NE exploitable block, chemical analyses of nodules were performed at 20 boxcorer stations. Comparison of the mean values of the metal contents from the laboratories of UCHT, Prague, Czech Republic (Vu et al., 2020) and SGIDŠ, Spišská Nová Ves, Slovakia (Mackových and Lučivjanský, 2020) are presented in Tab. 9. The coefficient of variation for each of the metals does not exceed 20 %, which means that the obtained data are homogeneous. Using the Mn/Fe module, as well as the productivity index ΣNi, Cu, Co, the nodule genotype was associated with each station (sample).

Tab. 9

Mean values of the contents of basic metals from the laboratories of the UCHT and SGIDŠ (20 stations of the H22_NE block).

n = 20	Mn [%]	Fe [%]	Ni [%]	Cu [%]	Co [%]	Zn [%]	Mo [%]	Pb [%]	Mn/ Fe ratio	ΣNi, Cu, Co [%]
UCHT	26.99	5.78	1.27	1.20	0.18	0.15	0.05	0.03	4.85	2.65
SGIDŠ	31.34	6.15	1.06	1.05	0.15	0.13	0.06	0.02	5.31	2.27

Tab. 10 presents the contents of 14 rare earth elements (without scandium and yttrium) in 20 nodule samples collected in the H22_NE exploitable block.

Chemical composition of nodules at particular stations allowed to determine genotypes within sampled blocks (H22_NE, PRZ and H33). Among samples, collected during expedition IOM-2019, diagenetic nodules occur at 18 stations, hydrogenetic at 5 stations and mixed type at 5 stations. Buried nodules were found at 11 box core stations. The results were added to those, which have been obtained during former expeditions.

Tab. 10

Mean values of REEs contents from the laboratories of the UCHT and SGIDŠ (20 stations of the H22_NE block).

n = 20	La	Ce	Pr	Nd	Sm	Eu	Gd	Tb	Dy	Ho	Er	Tm	Yb	Lu
	LREEs [ppm]							HREEs [ppm]						
UCHT	96.5	235	28.7	125	32.0	8.46	29.8	4.81	24.9	4.82	13.3	1.89	12.4	1.88
SGIDŠ	82.3	191	29.7	115	28.3	7.68	23.2	5.17	26.2	4.52	11.4	2.08	11.9	1.72

Geotechnical properties

The basic physical properties, which have to be determined on board immediately after the nodules are retrieved from the boxcorer or dredge samplers, are water content and bulk density (volumetric density). In addition, some other properties, such as dry nodule density (the drying takes place 72 hours at 105 °C), porosity, void ratio, and specific nodule density are calculated. Natural water content (ore based water content, w_n) is the ratio of the mass of evaporated water to the mass of wet nodule specimen. While the water content (w) and the natural water content (wn) analysis, the salt content in the sea water present in the nodule pores, assumed as M = 35 ‰, needs to be taken into account. Basic physical parameters of PMN investigated by IOM during the contract period are presented in Tab. 11.

Nodule blanketing in H22 exploration block and H22_NE exploitable block

Nodule blanketing (rate of sediment coverage, dimensionless coefficient) by the sediment is a characteristic feature of the entire IOM exploration area. Blanketing coefficient is calculated as the ratio of template coverage to seabed image coverage. If there is no sediment cover, the coefficient is 1. According to analysis of 76 samples (values of template and seabed photo) the mean value of blanketing coefficient for exploration block H22 is 1.3 (Zarzecki et al., 2021). H22_NE exploitable block average blanketing coefficient was calculated on 40 samples and represents value 1.3 as well (IOM, 2021).

Wet nodule abundance (kg/m^2) and nodule coverage (based on seabed photo in %) of 20 samples obtained during the IOM-2019 expedition were assessed. The positive correlation appears to be fairly strong (coefficient of determination R^2 = 0.66), giving evidence of similar level of nodule blanketing within the particular ore bodies (Fig. 17). It is clearly seen at the chart that about 50 % of nodule coverage on seabed photos corresponds to 14–20 kg/m^2 in boxcorer. Furthermore, if nodule coverage exceeds 60 %, nodule abundance about 20 kg/m^2 can be anticipated (Zarzecki et al., 2021).

Use of seafloor photographs for resources estimation

The main objective of the study (Mucha et al., 2020) was to assess the ability to determine polymetallic nodule abundance based on seafloor photography in the H22 exploration block of the IOM area. The assessment of the nodule abundance (APN) requires quality photographs of

Tab. 11

Basic physical parameters of nodules in the IOM exploration area in respect to the cruises 2001–2019 (values in a counter: min-max, value in a denominator: mean, n = number of analysis).

Year of the cruise	Water content, w [%]	Bulk density, ρ [g/cm^3]	Dry nodule density, ρ_d [g/cm^3]	Porosity, n [%]	Void ratio, e	Specific nodule density, ρ_s [g/cm^3]	Natural water content, w_n [%]
2001 n = 227	38–69 **47**	1.70–2.06 **1.95**	1.01–1.50 **1.33**	55–68 **60**	1.21–2.15 **1.53**	3.08–3.75 **3.35**	28–41 **32**
2004 n = 308	38–63 **48**	1.77–2.08 **1.95**	1.09–1.50 **1.31**	54–69 **62**	1.18–2.18 **1.62**	3.13–3.65 **3.43**	28–39 **33**
2009 n = 173	36–57 **46**	1.83–2.06 **1.97**	1.18–1.51 **1.35**	53–66 **61**	1.14–1.96 **1.57**	2.98–3.68 **3.46**	27–37 **32**
2014 n = 205	29–71 **47**	1.77–2.27 **1.97**	1.03–1.75 **1.34**	46–72 **62**	0.86–2.56 **1.62**	3.05–3.68 **3.49**	22–42 **32**
2019 n = 92	40–67 **48**	1.74–2.13 **1.99**	1.15–1.48 **1.35**	53–76 **63**	1.15–3.15 **1.70**	2.58–4.88 **3.65**	29–40 **32**

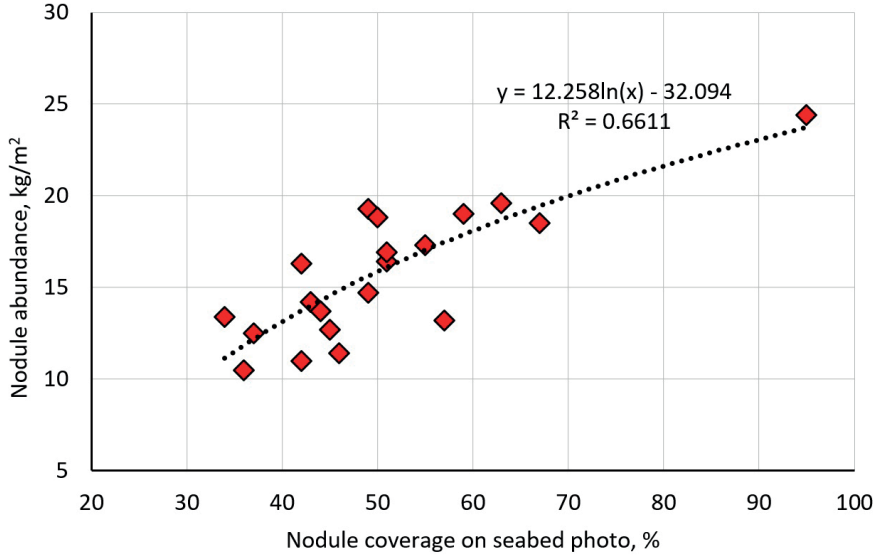

Fig. 17. Relation between nodule abundance and nodule coverage in H22_NE exploitable block (Zarzecki et al., 2021).

seafloor areas where the degree of covering nodules with bottom sediments is low. The measurement of the seafloor nodule coverage and basic geometrical features of the nodules: surface, long and short axes, and the number of nodules, should be carried out using well-sized images.

Out of 52 sampling sites (including photos), 37 were properly sized and used for analysis. The basic data set was insufficient to isolate large enough training and test sets (with at least 30 observations), respectively. For this reason, the cross-validation obtained is considered preliminary and requires additional verification on a bigger data set.

The created data sets, depending on the type and number of measured variables, were used to estimate the nodule abundance based on the equations of regression models. All analysed models are statistically significant at the significance level of 0.05. The accuracy of the estimation was quantified using the standard estimation error (SEE) and mean absolute estimation error (MAE).

All tested models are preliminary and require verification of their reliability based on a separate, independent and sufficiently large data set (> 30 observations). The best results were achieved with multivariate regression model using 8 variables (SEE = 2.53; MAE = 1.75):

$$\begin{aligned} APN\ [kg/m^2] = {} & 0.233 \cdot NCS[\%] - 0.002 \cdot NS + \\ & + 1.879 \cdot Mean\ A\ [cm] - 2.181 \cdot Median\ A\ [cm] + \\ & + 12.863 \cdot Mean\ La\ [cm] - 0.509 \cdot Median\ La\ [cm] - \\ & - 21.477 \cdot Mean\ Sa\ [cm] + 5.793 \cdot Median\ Sa\ [cm], \end{aligned}$$

where: NCS – percentage of seafloor nodule coverage, NS – number of nodules on the seafloor, Mean A – mean of nodule area, Median A – median of nodule area, Mean La – mean of long axis, Median La – median of long axes, Mean Sa – mean of short axis, Median Sa – median of short axis.

Combining measurements of the nodule abundance based on box corer data and seafloor photographs shall require the development of formulas taking into account the diverse geometrical bases of both types of data and the accuracy of determining the nodule abundance based on box corer sampling and the regression model.

Wasilewska-Błaszczyk & Mucha (2022) assessed possibilities and limitations of the use of seafloor photographs for estimating PMN resources in case study. Direct seafloor sampling is insuficient to obtain an acceptable accuracy of resource estimates in small blocks of potential deposits. This is why the results of photographic surveys of the seafloor are analysed to increase the reliability of the estimates.

A statistically significant correlation was found between the abundance of nodules and seafloor nodule coverage (quantitative variables), the nodule abundance and genetic type of nodules (ordinal variable estimated visually from photos), and between seafloor coverage with nodules and sediment coverage of nodules (ordinal variable estimated visually from photos). The correlation relationship between the seafloor nodule coverage determined manually and automatically (using computer software) was examined for the part of the data set (data from IOM-2014 expedition). A very strong linear correlation between the seafloor nodule coverage determined manually and automatically, with the correlation coefficient 0.966 (R2 = 93.3 %) was found.

Type and method of data collection (quantitative or ordinal) based on direct sampling and seafloor photographs is shown in Fig. 18. The values of the basic statistical parameters of nodule abundance (APN), seafloor coverage with nodules in the photograph (NC-S), and nodule coverage of the grid (NC-T) are summarized in Tab. 12.

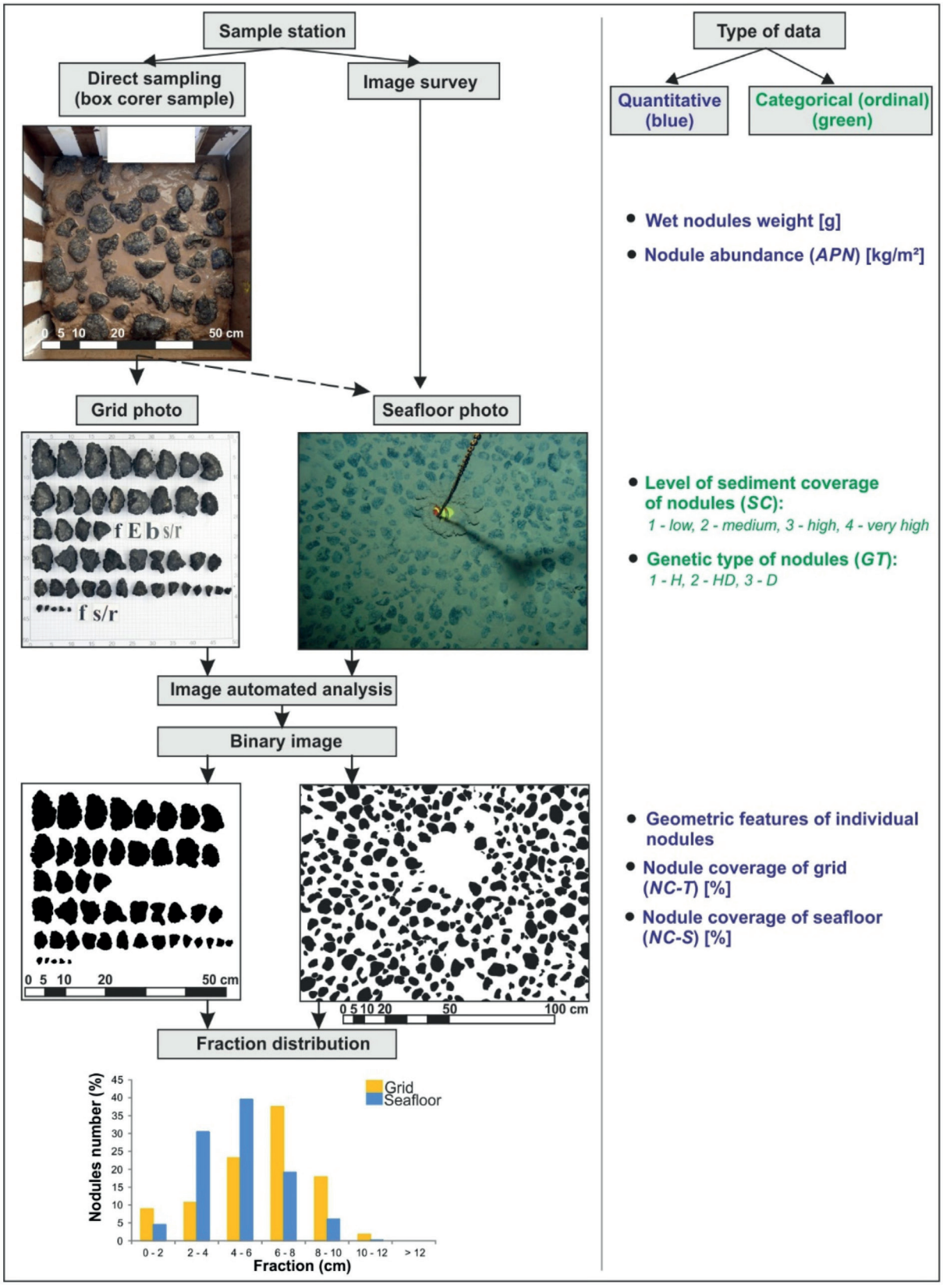

Fig. 18. Type and method of data collection (quantitative or ordinal) based on direct sampling and seafloor photographs (Wasilewska-Błaszczyk & Mucha, 2022).

Tab. 12

Statistics of nodule abundance (APN) and nodule coverage of laboratory grid (NC-T) and seafloor (NC-S).

Parameter	Expedition	Count	Minimum	Maximum	Arithmetic Mean	Standard Deviation	Coefficient of Variation	Skewness	Standard Skewness	Standard Curtosis
APN [kg/gm²]	2014	48	1.5	19.3	12.5	4.4	35.3	–0.62	–1.76	–0.23
	2019	20	6.9	23.1	15.9	4.4	27.9	–0.19	–0.35	–0.68
	2014 + 2019	68	1.5	23.1	13.5	4.6	34.4	–0.38	–1.29	–0.10
NC-T [%]	2014	48	5.2	63.2	41.4	12.5	30.1	–1.08	–3.04	2.02
	2019	20	24.0	70.0	55.0	10.7	19.4	–1.03	–1.88	2.18
	2014 + 2019	68	5.2	70.0	45.4	13.4	29.6	–0.80	–2.70	1.87
NC-S [%]	2014	48	7.0	72.0	37.9	13.3	35.1	–0.37	–1.06	0.56
	2019	20	18.0	59.0	43.3	10.3	23.7	–1.00	–1.82	1.02
	2014 + 2019	68	7.0	72.0	39.5	12.6	32.0	–0.56	–1.89	0.77

To estimate the nodule abundance at seafloor photographic stations where no samples were collected, statistical methods of multiple regression can be used, including general linear models, taking into account both – quantitative variable (percentage of seafloor nodule coverage) and categorized ordinal variables (degree of seafloor coverage with sediments, genetic type of nodules). Preliminary multiple regression analysis aimed at estimating nodule resources as a function of the percentage coverage of the seafloor with nodules, visual assessment of the coverage with bottom sediments (performed by a geologist experienced in the photographic evaluations), and the genetic type of nodules yielded promising results.

It should be noted that, contrary to expectations, the expansion of box corer dataset by adding a large amount of photographic data does not lead to a radical improvement of the accuracy of resources estimations. This is due to the very unfavorable linear distribution of photographic sites located only along the photo profiles, which is also reflected in the very uneven data distribution in individual smaller blocks (future mining fields). A significant accuracy improvement of PN resources estimations may be expected after taking the additional seafloor photographs along the lines perpendicular to the courses of the current photo profiles. Such opportunity is provided by the autonomous underwater vehicles (AUV). The additional exploration of the PN deposit will also be of great importance to evaluation of local variability and continuity of nodules abundance (Mucha & Wasilewska-Błaszczyk, 2022).

Estimation of resources

Current resources estimation is based on data collected during scientific expeditions carried out by IOM. So far, four reports using geostatistical data analysis have been prepared (2007, 2011, 2015 and 2020) and two validations performed by the Competent Person (2016 and 2020). The current state is shown in Tab. 13. The resource validation was carried out in accordance with the CRIRSCO directives (Committee for Mineral Reserves International Reporting Standards) and Annex V of the Recommendations for the guidance of contractors on the content, format and structure of annual reports (ISBA/21/LTC/15): Reporting standard of the International Seabed Authority for Mineral Exploration Results Assessments, Mineral Resources and Mineral Reserves (Szamałek, 2020). The effective date for the estimate is August 2020. No mineral reserves were estimated at this stage of the project development.

New estimation of mineral resources in B2 sector was caried out using the geostatistical method of ordinary block kriging with Yamamoto correction. Estimates of resources and abundance of nodules and metals were carried out in square elementary blocks with a side of 500 m using kriging and co-kriging (Fig. 19). The estimates used 8 nearest sampling stations, two from each quadrant (quarters) into which the circular data search zone was divided. The center of the circular data search zone coincides with the center of the elementary block. In the calculation procedure, isotropic models of variograms, cross-variograms,

Tab. 13

Mineral resource estimate of wet polymetallic nodules in the IOM Exploration Area. Cut-off 10 kg/m^2 of wet nodules – without volcanoes, seabed areas free of nodules and areas sloped over 7°. Note: Sector B2 includes exploration blocks H11, H22, H33, H44 and exploitable block H22_NE (Mucha & Wasilewska, 2007; Shanov et al., 2007; Mucha & Wasilewska-Błaszczyk, 2020; Szamałek, 2020).

Mineral Resource Classification	Mean Abundance [kg/m^2]	Mn [%]	Ni [%]	Cu [%]	Co [%]	Zn [%]	REE [ppm]	Resources Wet [Mt]
Measured (H22_NE block)	14.60	29.19	1.31	1.25	0.18	0.15	713	12.2
Measured Total								12.2
Indicated (H11 + H22 blocks)	12.40	31.37	1.30	1.29	0.16	0.16	–	77.0
Indicated Total								77.0
Inferred (B1 sector)	13.40	27.80	1.20	0.90	0.20	–	–	62.6
Inferred (H33 block)	12.00	32.35	1.41	1.20	0.18	0.15	–	21.8
Inferred (H44 block)	11.50	30.71	1.32	1.19	0.19	0.14	–	13.6
Inferred (B2 sector other)	11.59	30.90	1.32	1.21	0.18	0.15	–	85.3
Inferred Total								183.3
Grand Total								272.5

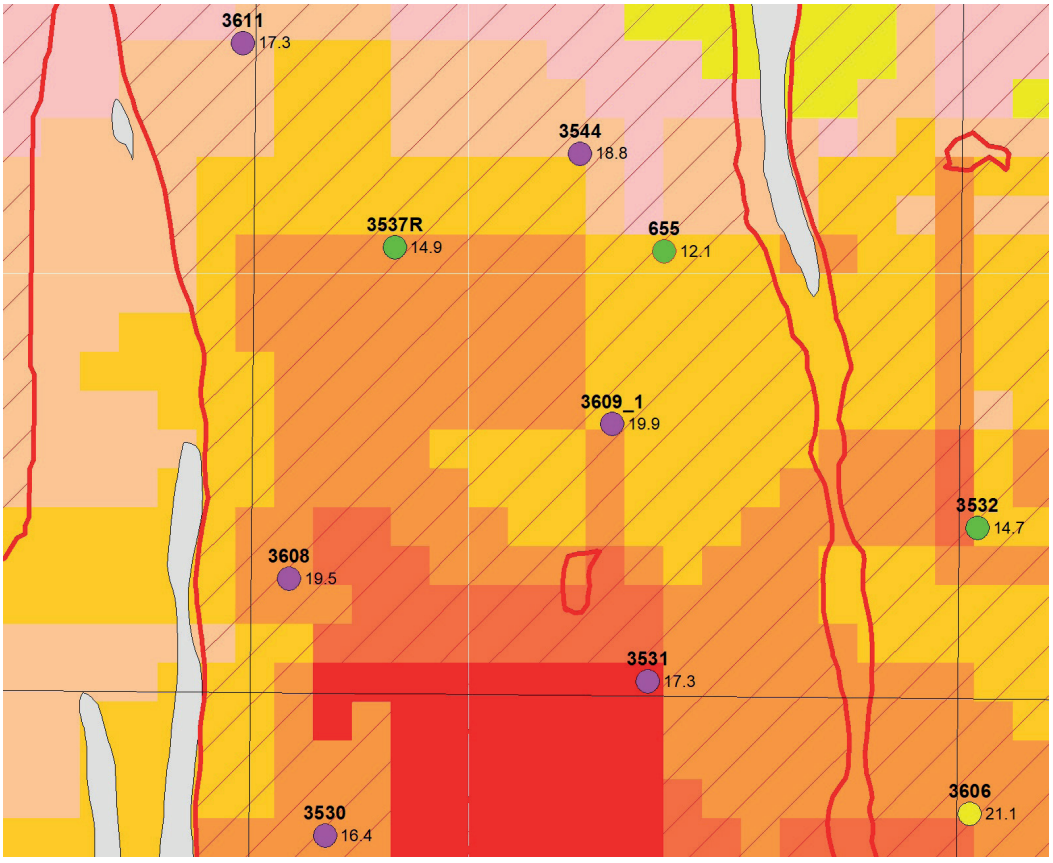

Fig. 19. Section from the most promising area of nodule abundance in H22_NE exploitable block. Grey areas represent seafloor with slope more than 7°, hatched areas represent ore bodies (Mucha & Wasilewska-Błaszczyk, 2020).

covariance and cross-co-variance were used. The total resources of polymetallic nodules of the exploration blocks and ore fields (ore bodies), for different values of maximal the ocean-floor slopes, were obtained by summation of resources estimated for elementary blocks.

The accuracy of resource estimation in blocks H11 + H22 and in block H22_NE is high as evidenced by small, standard kriging errors in the range of 3–6 %. The resources of nodules in blocks H33 and H44, expressed by standard errors from the 8–12 % range, were estimated with much lower accuracy. The different size of errors is the result of the different density of the bottom sampling in individual blocks.

The dependency of the tonnage of nodules and mean abundances in relation to the minimum abundance of wet nodules in B2 Sector is shown in Fig. 20.

Conclusions

Research work in the second phase of the deposit exploration included processing of data collected during the IOM-2019 expedition and combined with data sets from previous sampling campaigns (2001–2014). The analytical work was based on sediment and nodule analyses of samples from the H22 exploration block and the H22_NE exploitation block. The structure of the sedimentary cover of the H22 exploration block, grain size analysis, mineral analysis, physical, strength, geochemical and geotechnical properties of bottom sediments and nodules were studied. Chemical composition and the contents of all main metals, including REEs, were analysed. Continued work on use of seafloor photographs for resources estimation.

IOM has sufficient samples of adequate quality and authenticity to define Inferred, Indicated and Measured Mineral Resources. The effective date for the estimate is August 2020. Mineral Resources were estimated at various nodule abundance cut-offs. Selected base scenario is an abundance cut-off of 10 kg/m^2 (in wet condition). Metals of value are manganese, nickel, cobalt, copper, zinc and REEs. Other metals of potential value (Mo, Fe, Li) have not been estimated, but in the future, based on processing technology development, they could provide added value to the project.

Measured Resources in exploitation block H22_NE and Indicated Resources in exploration blocks H11 and H22 were selected for the Pre-feasibility Study. Future activities of IOM will focus on a detailed survey of selected blocks and increasing the category of resources, alternatively reserves. Geological data, together with other data obtained during the technological research of mining and processing methods, as well as environmental research represent the basis for the commercial model of deposit utilization. Legal framework for mining and environmental

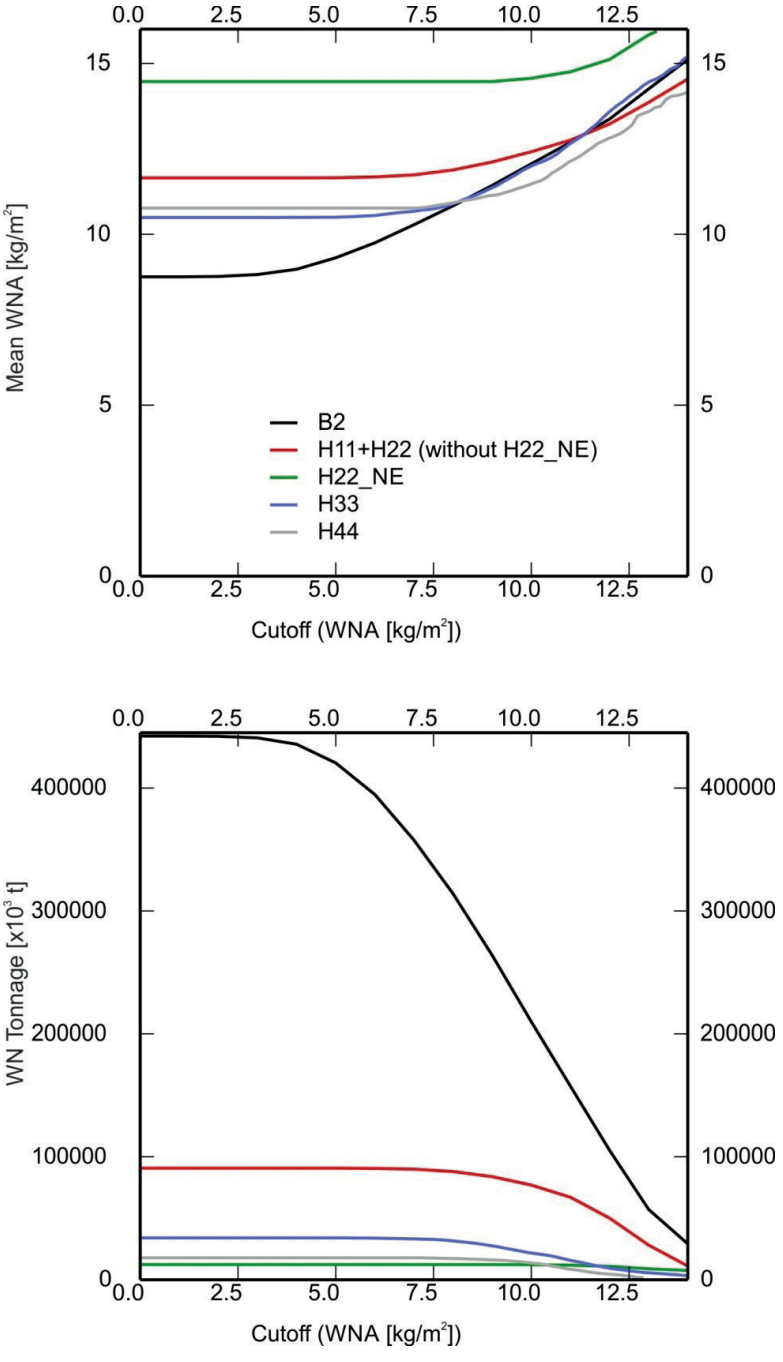

Fig. 20. Graph of the dependence of the average abundance of wet nodules (top) and the tonnage of wet nodules (bottom) on the cut-off value of the abundance of wet nodules (WNA); seabed slope ≤ 7° (Mucha & Wasilewska-Błaszczyk, 2020).

regulations, as a fundamental condition for future deep sea mining activities, is under the development by the ISA.

References

Baláž, P., Dreiseitl, I., Abramowski, T., Shiryaev, B., Cabello, M. & Mianowicz, K., 2019: Preliminary Economic Assessment Technical Report – IOM Polymetallic Nodules Project in CCZ, Pacific Ocean. *IOM Internal Report. Szczecin, IOM.*

Baláž, P., 2021: Results of the first phase of the deep-sea polymetallic nodules geological survey in the Interoceanmetal Joint Organization licence area (2001–2016). *Miner. Slov., 53, 1, 3–36.*

Dreiseitl, I., 2018: Otchet o kompleksnych geologo-ekologicheskich issledovanijach, vypolnennych v rejse IOM-2014 (in Russian language). *IOM Internal Report.*

IOM Report on Activities of the Interoceanmetal Joint Organization (IOM) in 2021 submitted in fulfilment of the Contract for Exploration concluded with the International Seabed Authority. *IOM Internal Report. Szczecin, 29 p.*

ISA, 09/2021: International Seabed Authority, Exploration Contracts (https://www.isa.org.jm/exploration-contracts).

ISA, 2021: International Seabed Authority, Polymetallic Nodules Exploration Areas (https://www.isa.org.jm/polymetallic-nodules-exploration-areas-clarion-clipperton-fracture-zone).

ISBA/21/LTC/15, 2015: International Seabed Authority, Recommendations for the guidance of contractors on the content, format and structure of annual reports (https://www.isa.org.jm/document/isba21ltc15).

Kowalska, S., 2014. Wyznaczanie zawartości substancji amorficznej w skałach metodą Rietvelda (XRD). *Nafta-Gaz, LXX, 10, 700–706.*

Maciąg, Ł., Kotliński, R. A. & Borówka, R. K., 2011: Lithological Variability of Siliceous Clayey Silts from IOM Area (Clarion-Clipperton Fracture Zone, East Pacific). *Gór. Geoinż., 35, 4, 243–255.*

Maciąg, Ł. & Zawadzki, D., 2019: Spatial variability and resources estimation of selected critical metals and rare earth elements in surface sediments from the Clarion-Clipperton Fracture Zone, equatorial Pacific Ocean, Interoceanmetal claim area. In: The 20th Annual Conference of the International Association for Mathematical Geosciences IAMG2019. *Pennsylvania, USA, St. College, 174–178.*

Maciąg, Ł., Zawadzki, D., Radziejewska, T., Wróbel, R., Sławińska, J., Osóch, P., Tomkowiak, J., Witkowski, J., Stachowska, Z., Januszkiewicz, A. & Tomaszewicz, A., 2020: Comprehensive analysis (chemistry, lithology, mineralogy, granulometry) of ocean floor sediments (IOM cruise 2019). Mar Ecol Consulting Teresa Radziejewska. *IOM Internal Report. Szczecin, 30 p.*

Maciąg, Ł., 2021: Comprehensive analysis (chemistry, lithology, mineralogy, granulometry) of ocean floor sediments (IOM cruise 2019), the complex SEM-EDX analyses. Mar Ecol Consulting Teresa Radziejewska. *IOM Internal Report. Szczecin, 64 p.*

Mackových, D. & Lučivjanský, P., 2020: Determination of matrix composition of polymetallic nodules on samples taken in the cruise IOM-2019. State Geological Institute of Dionýz Štúr, Geoanalytical laboratories. *IOM Internal Report. Szczecin, 21 p.*

Mucha, J. & Wasilewska, M., 2007: Estimation of polymetallic nodule resources of the IOM's exploration area and its nickel, manganese and molybdenum contents using a geostatistical method for available geological data processing (in Russian). *IOM Internal Report. Szczecin.*

Mucha, J., Wasilewska-Błaszczyk, M. & Yubko, V., 2011: Estimation of polymetallic nodule resources of and its nickel, manganese copper and cobalt contents using the geostatistical method of processing based on the IOM geological data. *IOM Internal Report. Szczecin.*

Mucha, J. & Wasilewska-Blaszczyk, M., 2020: Estimation of the Resources of Polymetallic Nodules and Contained Metals in Sector B2 and the Exploration Blocks H11 + H22, H33 and H44. *IOM Internal Report. Krakow, AGH Univ. Sci. Technol.*

Shanov, S., Boikova, A. & Radulov, A., 2007: Estimation of the resources of polymetallic nodules of the IOM exploration area and their content of copper, cobalt and zinc using a geostatistical method for processing the geological data available in IOM. *IOM Internal Report. Szczecin, 48 p.*

Skowronek, A., Maciag, Ł., Zawadzki, D., Strzelecka, A., Baláž, P., Mianowicz, K., Abramowski, T., Konečný, P. & Krawcewicz, A., 2021: Chemostratigraphic and Textural Indicators of Nucleation and Growth of Polymetallic Nodules from the Clarion-Clipperton Fracture Zone (IOM Claim Area). *Minerals, 11, 868,* https://doi.org/10.3390/min11080868.

Szamałek, K., 2020: Validation of the Estimation of Resources of Polymetallic Nodules and Metals Contained in the Nodules in the B2 Sector and Exploration Blocks H11, H22, H33 and H44 with Resource Categorization within the Seabed Exploration Area According to Agreement between IOM and the International Seabed Authority. *IOM Internal Report. Szczecin.*

Vu, H., Kristianová, E., Frýdl, T., Bastl, T., Tomaško, T. & Dvořák, P., 2020: Chemical analysis of nodule samples recovered during the IOM-2019 cruise. University of chemistry and technology, Faculty of Chemical Technology, Prague. *IOM Internal Report. Szczecin, 50 p.*

Zarzecki, D., Kołodziejczyk, M., Hendryk, M., Urbanek, M., Abramowski, T., Baláž, P., Cabello, M., Dreiseitl, I., Mianowicz, K. & Shiryaev, B., 2021: Pre-Feasibility Study Technical Report on the IOM Polymetallic Nodules Project in Clarion-Clipperton Zone. *IOM Internal Report. Szczecin, 328 p.*

Zawadzki, D., Maciąg, Ł., Abramowski, T. & McCartney, K., 2020: Fractionation Trends and Variability of Rare Earth Elements and Selected Critical Metals in Pelagic Sediment from Abyssal Basin of NE Pacific (Clarion-Clipperton Fracture Zone). *Minerals, 10, 4.*

Výsledky druhej fázy geologického prieskumu hlbokomorských polymetalických konkrécií v prieskumnom území Spoločnej organizácie Interoceanmetal (2016 – 2021)

Prieskumné práva boli Spoločnej organizácii Interoceanmetal udelené na prieskum polymetalických konkrécií (PMN) 29. marca 2001 na území nachádzajúcom sa v zóne Clarion-Clipperton (CCZ) vo východnej časti centrálneho Tichého oceánu. Prieskumné územie má rozlohu približne 75 000 km^2 a pozostáva z dvoch sektorov (B1 a B2). Sektor B2 zahŕňa štyri prieskumné bloky (H11, H22, H33 a H44). Najperspektívnejšia oblasť vybraná na podrobný prieskum je označená ako H22_NE (*exploitable block*) a *je* vymedzená v rámci prieskumného bloku H22. V článku sú uvedené výsledky geologického prieskumu na základe dát získaných počas druhej fázy prieskumu (2016 – 2021, t. j. prvé predĺženie zmluvy na prieskum). Výsledky sú založené na dátach z expedícií IOM a príslušných analytických prácach. Počas expedície IOM-2018 sa uskutočnil batymetrický prieskum prieskumných blokov H11, H22, H33 a H44. Expedícia IOM-2019 poskytla nový súbor údajov získaných pomocou dištančných metód (sonár s bočným skenovaním, *profiler*) a kontaktných metód (*box-corer* a *gravity-corer*) v bloku H22_NE, prieskumnom bloku H33 a predbežne vymedzenej ochrannej referenčnej zóne (PRZ). Ochranná referenčná zóna (*Preservation Reference Zone*) je oblasť, v ktorej sa nesmie vykonávať ťažba, aby sa zabezpečila reprezentatívna biota morského dna s cieľom porovnania zmien morského prostredia s územím ťažby. Povinnosť stanoviť PRZ vo svojom prieskumnom území ukladá vykonávateľovi prieskumu ISA (*International Seabed Authority* – Medzinárodná organizácia pre morské dno).

Výsledkom batymetrických prác bol súbor nových máp povrchu morského dna vrátane vrstevnicovej mapy, mapy sklonov morského dna, ako aj mapy amplitúd spätne rozptýleného signálu (*backscatteru*). Prieskumné bloky boli zmapované v mierke 1 : 100 000, detailne mapovaný blok H22_NE v mierke 1 : 50 000. Štúdium štruktúry sedimentárneho pokryvu prieskumného bloku H22 bolo založené na interpretácii hydroakustického profilu s vymedzením jednotlivých sedimentárnych komplexov, resp. subkomplexov a bazaltového podložia.

Analytické práce boli založené na analýzach vzoriek sedimentov a konkrécií z bloku H22 a H22_NE. Skúmala sa štruktúra sedimentačného pokryvu prieskumného bloku H22, vykonala sa analýza granulometrie, minerálna analýza, fyzikálne, pevnostné, geochemické a geotechnické vlastnosti sedimentov dna a polymetalických konkrécií. Analyzovalo sa chemické zloženie a obsah všetkých hlavných kovov vrátane REE. Použité postupy zahŕňali širokú škálu analytických metód (XRD, XRS, XRF, SEM/EDX, EPMA BSE, FAAS, ICP-MS, ICP-AES). Bola navrhnutá aj hypotéza prirodzeného praskania (deštrukcie) konkrécií na morskom dne vyvolaného vnútorným napätím v žilách, iniciovaného diagenézou sedimentov v dutinách a následne rastom kryštálov v cementačnej výplni trhlín.

Pokračovali práce na využívaní fotografií morského dna na odhad zdrojov/zásob polymetalických konkrécií. Hlavným cieľom štúdia bolo posúdenie schopnosti určiť hustotu uloženia (kg/m^2) konkrécií na základe analýzy fotografií morského dna v prieskumnom bloku H22. Odhad hustoty uloženia konkrécií si vyžaduje kvalitné fotografie oblastí morského dna a nízku mieru pokrytia konkrécií sedimentmi dna. Meranie základných geometrických parametrov konkrécií prebiehalo manuálne, ako aj s využitím softvéru na analýzu obrazu. Bol pripravený multivariačný regresný model na orientačný výpočet hustoty uloženia na základe geometrických parametrov konkrécií získaných z fotografii morského dna.

Výsledky prieskumu boli po jednotlivých expedíciách zhrnuté v správach o geologickom a environmentálnom výskume, v polročných správach na zasadnutia Rady IOM, ako aj vo výročných správach pre ISA. Prehľad a výsledky prieskumných prác boli zhrnuté v technických správach (Baláž et al., 2019; Zarzecki et al., 2021). Prezentované výsledky poskytujú dodatočné informácie k už skôr publikovaným údajom (Baláž, 2021), ktoré sú relevantné na aktualizáciu odhadu zdrojov v sektore B2. Získané údaje a analýzy sa využívajú pri plánovaní projektu využívania polymetalických konkrécií IOM.

Nový odhad zdrojov v sektore B2 bol vykonaný pomocou geoštatistickej metódy blokového krigingu s Yamamotovou korekciou. Zdroje polymetalických konkrécií boli zaradené do kategórií *Inferred*, *Indicated* a *Measured* podľa klasifikačného systému CRIRSCO. Súčasný odhad množstva zdrojov vychádza z údajov zhromaždených počas všetkých vedeckých expedícií. Doteraz boli vypracované štyri výpočty s použitím geoštatistickej analýzy údajov (2007, 2011, 2015 a 2020) a dve validácie vykonané kompetentnou osobou (2016 a 2020). Súčasný stav je uvedený v tab. 13. Validácia zdrojov bola vykonaná v súlade so smernicami CRIRSCO (Výbor pre medzinárodné

štandardy vykazovania zásob nerastných surovín) a ISA (ISBA/21/LTC/15: *Reporting standard of the International Seabed Authority for Mineral Exploration Results Assessments, Mineral Resources and Mineral Reserves*). Dátum účinnosti posledného výpočtu zdrojov je august 2020. V tejto fáze projektu neboli odhadnuté žiadne zásoby nerastných surovín.

Nerastné zdroje boli odhadnuté pri rôznych hraničných hodnotách hustoty uloženia konkrécií. Zvolený základný scenár používa medznú hodnotu (*cut-off*) 10 kg/m^2 (vo vlhkom stave). Hlavnými záujmovými kovmi sú mangán, nikel, kobalt, meď, zinok a REE. Ďalšie kovy s potenciálnou hodnotou (Mo, Fe, Li) neboli odhadnuté, ale v budúcnosti by na základe vývoja technológií spracovania mohli predstavovať pridanú hodnotu projektu.

Geologické údaje spolu s ďalšími údajmi získanými počas technologického výskumu ťažobných a spracovateľských metód, ako aj environmentálneho výskumu predstavujú základ komerčného modelu využívania ložiska. Právny rámec ťažby (vrátane environmentálnych predpisov) vypracúva ISA a je v štádiu prípravy.

Doručené / Received: 21. 11. 2022
Prijaté na publikovanie / Accepted: 15. 12. 2022